Effects of City Size on Thunderstorm Evolution Revealed through a Multiradar Climatology of the Central United States

DARREL M. KINGFIELD[a]

Cooperative Institute for Mesoscale Meteorological Studies, University of Oklahoma, and NOAA/OAR/National Severe Storms Laboratory, and Department of Geography and Environmental Sustainability, University of Oklahoma, Norman, Oklahoma

KRISTIN M. CALHOUN

Cooperative Institute for Mesoscale Meteorological Studies, University of Oklahoma, and NOAA/OAR/National Severe Storms Laboratory, Norman, Oklahoma

KIRSTEN M. DE BEURS

Department of Geography and Environmental Sustainability, University of Oklahoma, Norman, Oklahoma

GEOFFREY M. HENEBRY

Geospatial Sciences Center of Excellence, and Department of Natural Resource Management, South Dakota State University, Brookings, South Dakota

(Manuscript received 17 October 2016, in final form 7 November 2017)

ABSTRACT

Five years of 0.01° latitude × 0.01° longitude multiradar multisensor grids of composite reflectivity and vertically integrated signals from the maximum expected size of hail (MESH) and vertically integrated liquid (VIL) were created to examine the role of city size on thunderstorm occurrence and strength around four cities: Dallas–Fort Worth, Texas; Minneapolis–St. Paul, Minnesota; Oklahoma City, Oklahoma; and Omaha, Nebraska. A storm-tracking algorithm identified thunderstorm areas every minute and connected them together to form tracks. These tracks defined the upwind and downwind regions around each city on a storm-by-storm basis and were analyzed in two ways: 1) by sampling the maximum value every 10 min and 2) by accumulating the spatial footprint over its lifetime. Beyond examining all events, a subset of events corresponding to favorable conditions for urban modification was explored. This urban favorable (UF) subset consisted of nonsupercells occurring in the late afternoon/evening in the meteorological summer on weak synoptically forced days. When examining all thunderstorm events, regions at variable ranges upwind of all four cities generally had higher areal mean values of reflectivity, MESH, and VIL relative to downwind areas. In the UF subset, the larger cities (Dallas–Fort Worth and Minneapolis–St. Paul) had a 24%–50% increase in the number of downwind thunderstorms, resulting in a higher areal mean reflectivity, MESH, and VIL in this region. The smaller cities (Oklahoma City and Omaha) did not show such a downwind enhancement in thunderstorm occurrence and strength for the radar variables examined. This pattern suggests that larger cities could increase thunderstorm occurrence and intensity downwind of the prevailing flow under unique environmental conditions.

1. Introduction

The rate of urbanization by the global population is on an upward trend, from 30% in 1950 to 54% today, with two-thirds of the world projected to be living in urban areas by 2050 (United Nations 2014). Population redistribution concomitant with economic development is causing many cities across the world to experience an urban area

[a] Current affiliation: Cooperative Institute for Research in Environmental Sciences, University of Colorado Boulder, and NOAA/OAR/Earth System Research Laboratory, Boulder, Colorado.

Corresponding author address: Darrel Kingfield, darrel.kingfield@noaa.gov

DOI: 10.1175/JAMC-D-16-0341.1

expansion at more than double the rate of their respective population growth in the latter portion of the twentieth century (Angel et al. 2011). Expanding urban landscapes reduce local biodiversity and enhance surface roughness as a result of the spatial distribution of impervious surfaces (Landsberg 1981; Seto et al. 2012), modify the atmospheric contributions of aerosols (Van den Heever and Cotton 2007; Rosenfeld et al. 2008; Ntelekos et al. 2009; Schmid and Niyogi 2017), and alter surface energy budgets to generate urban heat islands (UHIs; Oke 1973, 1987). As a result, there is a continued demand to study the meteorological impacts, among other topics, caused by these urban-induced environmental feedbacks (Melillo et al. 2014).

Studies investigating the effects of urban environments on precipitation modification have been occurring for nearly a century (see reviews by Landsberg 1981; Lowry 1998; Shepherd 2005; Souch and Grimmond 2006; Shepherd 2013; Mitra and Shepherd 2016). One notable observational study, as summarized in Changnon (1968, 1980), suggested that Chicago, Illinois, is increasing the number of rainfall and hail hazard days in La Porte, Indiana. This study led to a seminal coordinated field program, the Metropolitan Meteorological Experiment (METROMEX), which explored inadvertent modification of precipitation patterns by the city of St. Louis, Missouri (Changnon et al. 1971). Results from this campaign revealed a 4%–25% increase in rainfall around 50–75 km downwind of the city during the warm season months (Changnon 1979; Changnon et al. 1991). METROMEX not only validated prior urban thunderstorm studies, it also served as the impetus for continued urban meteorological modification research across the United States (e.g., Westcott 1995; Bornstein and Lin 2000; Shepherd et al. 2002; Dixon and Mote 2003; Burian and Shepherd 2005; Niyogi et al. 2006 Mote et al. 2007; Ntelekos et al. 2007; Rose et al. 2008; Hand and Shepherd 2009; Niyogi et al. 2011; Ashley et al. 2012; J. A. Smith et al. 2012; Haberlie et al. 2015; Niyogi et al. 2017) and around the world (e.g., Yonetani 1982; Jauregui and Romales 1996; Tayanc and Toros 1997; Robaa 2003; Kishtawal et al. 2010; Mitra et al. 2012; Zhang et al. 2014; Dou et al. 2015; Singh et al. 2016).

Contemporary observational studies use a variety of tools and datasets to document inadvertent precipitation modification by urban areas. Many past approaches have relied on the measurement of precipitation at a single point or the assembly of observational points into a contour map (Huff and Changnon 1972; Jauregui and Romales 1996; Bornstein and Lin 2000; Burian and Shepherd 2005; Diem and Mote 2005; Niyogi et al. 2017). Using 19 rain gauges around the Houston, Texas, metro area, Burian and Shepherd (2005) found an increase in rainfall totals ranging from 59% within the urban footprint to 30% downwind of Houston between noon and midnight. Diem and Mote (2005) found an increase in the number of summertime heavy-precipitation days at a station 30 km downwind of Atlanta, Georgia, which they postulate is due to increased urbanization of the metropolitan area. In one part of Niyogi et al. (2017), they examined 50 years of gauge network data across the eastern United States and found that locations near urban–rural boundaries experienced significantly more rainfall in the summer months. While gauge networks serve as a direct measurement of the amount of rainfall, thunderstorms and their associated precipitation magnitudes can vary geographically, causing an underestimate in precipitation totals with a sparse observation network (Smith et al. 1994; Souch and Grimmond 2006).

The integration of satellite-based data has also been a relevant technique in recent years. Hand and Shepherd (2009) compared satellite-based radar from the Tropical Rainfall Measuring Mission (TRMM) Multisatellite Precipitation Analysis (TMPA) to rain gauges around Oklahoma City, Oklahoma (OKC). Not only did they observe a strong relationship between the prevailing wind and a rainfall enhancement in a 25-km area northeast of OKC, they also found that the satellite-based precipitation estimates were relatively accurate when compared to gauge networks. The global ubiquity of satellite data allows for the use of TRMM/TMPA data to explore the positive correlation between rapid urbanization and precipitation enhancement in India (Kishtawal et al. 2010; Mitra et al. 2012) and a measured decline in the number of precipitation days in Beijing, China (Zhang et al. 2014). However, because of its non-geostationary orbit, the TMPA system was unable to perform subhourly analyses, limiting its ability to collect precipitation information on individual thunderstorm events (Shepherd and Burian 2003).

The integration of terrestrial lightning detection networks partially addresses these temporal limitations by allowing for the identification of predominantly cloud-to-ground (CG) strikes across widespread areas at subminute temporal resolution [see the review by Stallins and Rose (2008)]. Urban aerosols can play a role in changing the microphysical processes associated with the strength and duration of updrafts (Van den Heever and Cotton 2007; Rosenfeld et al. 2008; Schmid and Niyogi 2017), and updraft strength is strongly correlated to total lightning production (Deierling and Petersen 2008). In the United States, Steiger et al. (2002) and Stallins et al. (2006) found enhanced CG lightning densities over and downwind of Houston and Atlanta, respectively. Yet,

CG lightning occurrence can be discontinuous in time and space, leading to challenges in making spatial associations with specific thunderstorms (Boussaton et al. 2007; Stallins and Rose 2008).

Ground-based radar provides a spatially continuous view of precipitation echoes and is a valuable tool for examining the urban feedbacks on thunderstorms (e.g., Matyas 2010). Atkinson (1971) used radar to track the echo position and intensity of a single thunderstorm and observed rapid cloud growth followed by a local precipitation maximum within the city limits of London, United Kingdom. Bornstein and LeRoy (1990) used radar reflectivity to show echo maxima over New York City, New York, associated with urban-initiated thunderstorms and highlight a propensity for storms that initiated upwind of the city to bifurcate after interacting with the city. In recent years, Doppler radar data, particularly from the Weather Surveillance Radar-1988 Doppler (WSR-88D) network, have been used to develop retrospectives of urban-induced thunderstorm initiation and intensity tracking (Mote et al. 2007; Niyogi et al. 2011; Ashley et al. 2012; Haberlie et al. 2015). Leveraging hourly precipitation data from the WSR-88D site collocated with Atlanta, Mote et al. (2007) observed precipitation enhancement downwind of the city that is most evident in the early evening hours through the summer months of 2002–06. Niyogi et al. (2011) evaluated 91 unique summertime thunderstorm events around Indianapolis, Indiana, and found that 60% of storms interacting with the city changed structure (i.e., shape and size), with these changes occurring more frequently during the daytime compared to nighttime convection. An accompanying model sensitivity analysis of a convective event run with the Indianapolis urban area present and absent reveals the urban-present case altered the atmospheric flow patterns significantly. This is likely due to the different surface characteristics in urban landscapes compared to rural areas. These include increased surface roughness, lower albedo, and elevated heat capacity due to the abundance of human-made materials. Ashley et al. (2012) evaluated 10 summers' worth of 5-min composite reflectivity data alongside CG lightning data to examine the influence of five urban and two rural areas in the southeastern United States on thunderstorm activity occurring on synoptically benign days. Their observations suggest that larger cities have a positive correlation to thunderstorm frequency and intensity while midsize cities provide a more muted signal that is difficult to decouple from other local or regional physiographical processes. Haberlie et al. (2015) used an extended version of the composite reflectivity dataset from Bentley et al. (2010) and Ashley et al. (2012) to examine how the urban environment around Atlanta affects the rate of isolated convective initiation (ICI) events. After segmenting to summer months and synoptically benign days, they found that ICI occurrence was most pronounced in the late afternoon/early evening hours (2100–0300 UTC), particularly during weekdays, compared to a rural control region west of the city. In addition, ICI occurrence tended to occur over and downwind of the city area, particularly for 700-hPa flows with a northerly component.

In general, most investigations using radar to understand urban-induced feedbacks have focused on summertime months when urban and rural temperature differences are the highest; however, these temperature differences exist year round (Gallo and Owen 1999). The few multiradar WSR-88D studies have focused on the southeastern United States (Bentley et al. 2010; Ashley et al. 2012; Haberlie et al. 2015) while observational studies outside this region have focused on single-radar analyses of reflectivity (Bornstein and LeRoy 1990; Niyogi et al. 2011) or rainfall (J. A. Smith et al. 2012) for one metropolitan area. Huff and Changnon (1973) found inadvertent precipitation modification around six cities, three of which (Chicago, St. Louis, and Cleveland, Ohio) were located in the central United States and displaced from the eastern seaboard where a majority of observational WSR-88D studies have occurred. Furthermore, several studies suggest that thunderstorm modification can lead to taller convective clouds, allowing for greater amounts of supercooled water to enter the $-10°$ to $-20°$C isothermal region, enhancing the potential for lightning and hail hazards (Shepherd 2005; Van den Heever and Cotton 2007). Yet, the ability to observe and calculate the vertically integrated signal of a radar echo is underexplored to date.

This study fills in some of the knowledge gaps above by first introducing how to use the Multi-Radar Multi-Sensor system (MRMS; Smith et al. 2016) framework to quality control and create 3D cubes of radar reflectivity and subsequently derive vertically integrated fields for precipitation volume and hail growth. Second, this workflow is used to create a 5-yr (2010–14), all season, MRMS dataset to examine thunderstorm frequency and strength around four cities of different sizes in the central United States: Dallas–Fort-Worth, Texas (DFW); OKC; Omaha, Nebraska (OAX); and Minneapolis–St. Paul, Minnesota (MSP). This region is not only underexplored in contemporary studies, but represents an area relatively sheltered from major physiographic factors (i.e., oceans and mountain ranges) that can influence thunderstorm activity and be difficult to decouple from urban influences (Ashley et al. 2012; Walker et al. 2015).

In addition to generating the MRMS framework, this study uses an automated thunderstorm identification and tracking system to identify thunderstorm areas (hereafter referred to as objects) and collect radar-derived attributes at

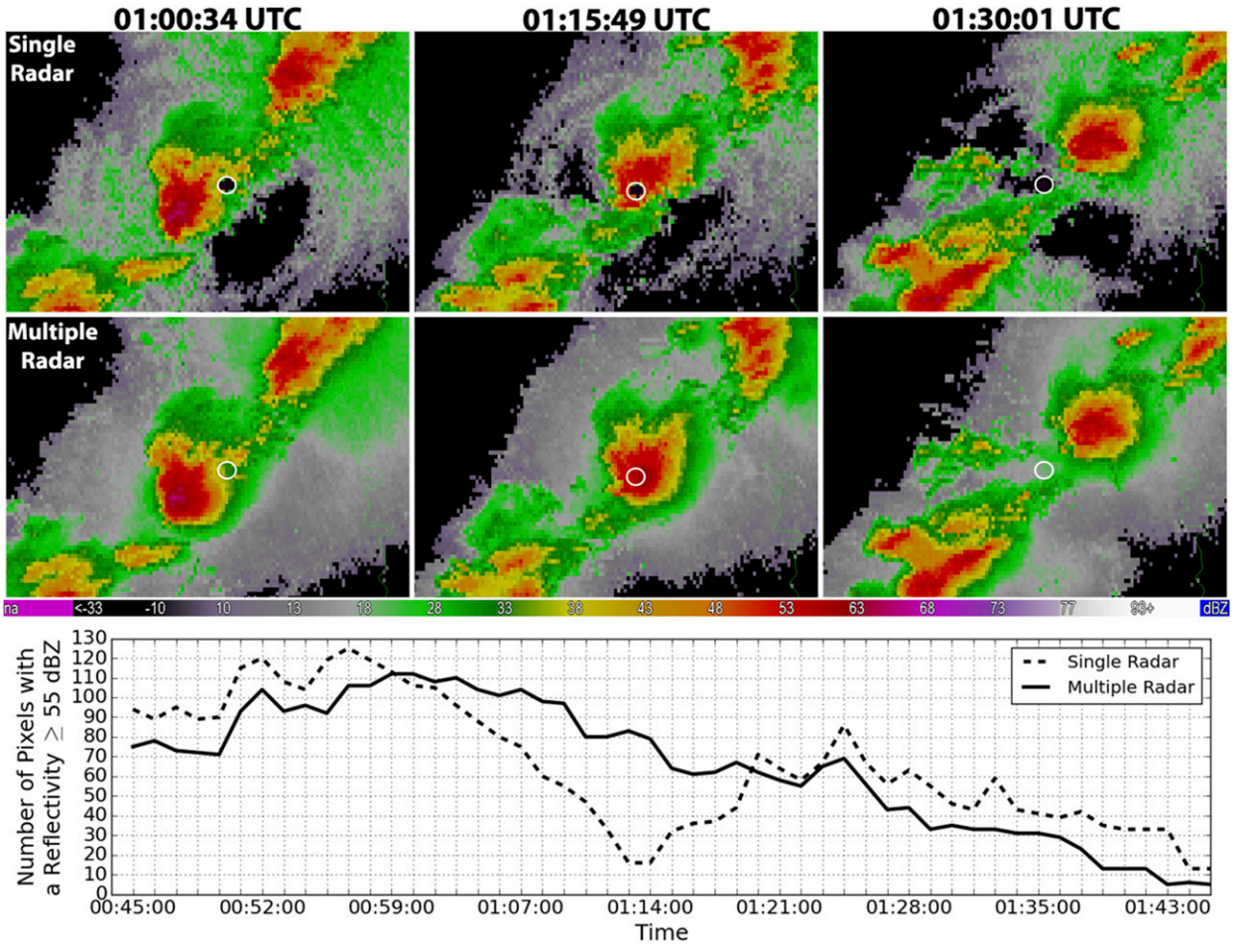

FIG. 1. Time series of the 55-dBZ echo area of a thunderstorm passing over the KOAX WSR-88D site (white circle) on 24 May 2012 derived from single- and multiple-radar analyses. In the single-radar analysis, there is an artificial decline in the echo area as the storm moves over the radar site as a result of sampling limitations. Leveraging data from multiple radars mitigates this issue and provides a cleaner evaluation of storm intensity.

each time step. Using these event-specific objects, the objective of this study will be to examine the role city size plays in the strength of a thunderstorm, expressed by using composite reflectivity (i.e., the maximum reflectivity measured in the vertical column), and the vertical structure and intensity of a thunderstorm, expressed using calculations of vertically integrated liquid (VIL; Greene and Clark 1972) and the maximum expected size of hail (MESH; Witt et al. 1998). VIL and MESH are two ways to represent the 3D structure of a precipitation echo in a 2D plane and have been used in recent examinations detailing the relationships between thunderstorm kinematics and lightning (e.g., Chronis et al. 2015; Schultz et al. 2015) and forecasting severe convective potential (e.g., Cintineo et al. 2014).

One of the primary benefits to using a multiradar blending approach over a single-radar analysis is that several WSR-88Ds are near urban areas and can underestimate intensity when a thunderstorm is nearby For instance, a convective cell passed directly over the KOAX WSR-88D site near OAX on 24 May 2012 (Fig. 1). Tracking intensity by the 55-dBZ echo area in composite reflectivity shows a rapid decline as the storm passes near and over the radar site before increasing again. MRMS, because of its ability to blend information from multiple radars to mitigate radar geometry issues, fills in the area over KOAX to provide better vertical coverage of the storm (Lakshmanan et al. 2006). As a result, the MRMS reflectivity dataset does not show this artificial rapid decline in thunderstorm intensity as was observed in the single-radar analysis. This improvement is very important given that a WSR-88D site exists within the urban footprint for two of the study cities (DFW and MSP), within 7 km from OAX, and 10 km from OKC.

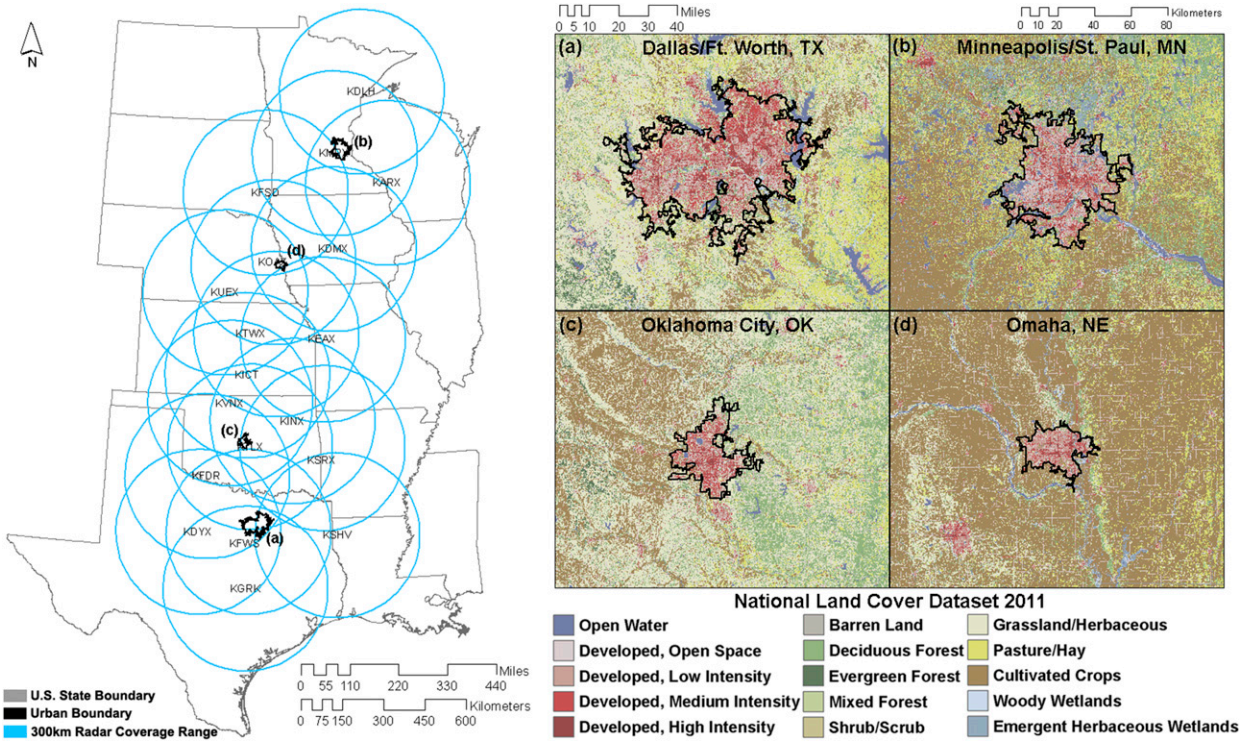

FIG. 2. The study domain covering 2 177 084 km^2 of the U.S. central plains. (left) The cities using the Topologically Integrated Geographic Encoding and Referencing (TIGER) dataset (black contours; U.S. Census Bureau 2010) and 300-km radar coverage regions utilized in this study (blue circles). (right) Land cover classification by the 2011 NLCD dataset around each of these cities.

2. Study domain

The study domain extends from 49.6°N, 102.5°W in the northwest corner to 28.0°N, 84.9°W in the southeast corner and encompasses a region commonly referred to as the U.S. Great Plains (Rossum and Lavin 2000) (Fig. 2). Four cities with different spatial urban footprints (Table 1) were chosen for analysis with the urban size ranging from 702.4 km^2 in OAX to 4607.9 km^2 in DFW. According to the 2011 version of the National Land Cover Database (Homer et al. 2015), four categories—shrub/scrub (52), grassland (71), pasture/hay (81), and cultivated crops (82)—constitute the majority of the land cover within 25 km of each city. These categories constitute 70.4% of the land cover surrounding DFW, 62.6% around MSP, 69.6% around OKC, and 83.7% around OAX. As described in Walker et al. (2015), mean annual precipitation rates decline westward toward the Rocky Mountains and along a southeast–northwest gradient across the Great Plains. As a result, the northern two cities see around a 150-mm decline in mean precipitation relative to the OKC and DFW domains. From 2010 through 2014, the SPC severe thunderstorm events database (Schaefer and Edwards 1999) shows at least 400 reports of significant severe hazards [i.e., hail $\geq$ 2 in. (1 in. = 25.4 mm), wind gusts $\geq$ 65 kt (1 kt = 0.51 m s^{-1}), or tornado] occurring within 200 km of each city. The ingredients for thunderstorms are more prevalent at southern latitudes, leading to an increased number of severe thunderstorm opportunities and reports in the southern two cities (e.g., Brooks et al. 2003; B. T. Smith et al. 2012; Cintineo et al. 2012).

3. Data

a. Radar data

The WSR-88D Next-Generation Weather Radar (NEXRAD) network, consisting of 160 S-band radars across the United States and outlying territories, was installed as part of the National Oceanic and Atmospheric Administration's (NOAA) National Weather Service (NWS) modernization and restructuring initiative in the 1990s with the goal of improving hazardous weather awareness and warning performance (Crum and Alberty 1993; Polger et al. 1994). Since its initial inception, numerous improvements in data quality control and resolution have been operationally implemented (Crum et al. 1998). This 5-yr study period represents one such era of improvement with the availability of ''superresolution'' products for all NEXRAD radars of interest (Torres and Curtis 2007).

TABLE 1. Population and land area from the 2010 U.S. Census (U.S. Census Bureau 2010), latitudinal and longitudinal length of the urban area defined using the 2011 NLCD dataset, twentieth-century mean annual precipitation from NOAA/NCEI (2014), and significant severe thunderstorm hazards inside the urban footprint and within 200 km of the urban footprint from 2010 to 2014 from the Storm Prediction Center events database (Schaefer and Edwards 1999).

City	Population	Land area (km^2)	Latitudinal length (km)	Longitudinal length (km)	Mean annual precipitation (mm)	Significant severe hazards within urban footprint	Significant severe hazards within 200 km of urban footprint
OAX	725 008	702	40	47	723	16	625
OKC	861 505	1064	56	53	874	55	658
MSP	2 650 890	2647	83	85	717	27	409
DFW	5 121 892	4608	103	127	869	86	578

Superresolution enhances the quality of base radar variables by reducing the effective scanning beamwidth from 1.38° to 1.02°. This allows for vortex and other storm-scale features to be resolved at longer ranges from any single WSR-88D (Brown et al. 2002, 2005).

A level-II archive of these data, containing at least three Doppler radar moments (i.e., reflectivity, velocity, and spectrum width) along with system status and interpretation information (Crum et al. 1993), is available for download from the National Centers for Environmental Information (NCEI). All available level-II data for each of the 19 WSR-88D sites from 2010 to 2014, amounting to 7 107 005 volume scans, were utilized in this study.

b. *Lightning data*

The NLDN is a system of ground-based lightning sensors that detects electromagnetic radiation emitted by CG flashes and strokes as well as a small percentage of in-cloud pulses across the continental United States (CONUS) (Cummins et al. 1998). Major network upgrades in 2003 provide uniform continental coverage with a high detection efficiency (~95%) for CG flashes and geographically variable detection efficiency for cloud flashes (16%–40%; Cummins and Murphy 2009). Using the National Severe Storms Laboratory NLDN archive, 1 234 625 one-minute time steps were downloaded to identify the 39 664 548 CG events that occurred in the study domain.

c. *Environmental analysis*

The Rapid Update Cycle (RUC; Benjamin et al. 2004) was the first operational numerical weather prediction system to assimilate multisensor observations and provide both hourly analysis (i.e., current conditions) and short-range forecast grids to enhance situational awareness on near-term hazardous weather. In 2012, the improvements to the RUC assimilation framework were implemented and the system was rebranded as Rapid Refresh (RAP; Benjamin et al. 2016). This study uses the hourly analysis fields produced by the RUC and RAP (hereinafter referred to as the model) to improve the dealiasing of radar velocity data (e.g., Miller et al. 2013), create blended radar and environmental fields (e.g., Smith et al. 2016), and assist in the classification of thunderstorm convective modes (e.g., Hobson et al. 2012). Five years of the highest-resolution model analysis data (either 20 or 13 km), amounting to 43 613 h, were downloaded from the NCEI National Model Archive and Distribution System. If an hourly analysis grid is missing, another grid up to 3 h old was used to fill in the missing values; otherwise, that hour was excluded from the dataset. This was mainly an issue between 1 and 8 May 2012, during the initial operational transition from RUC to RAP.

d. *Urban boundaries*

There is no standardized definition of urbanization in the past literature. Urban areas have been defined by circular search areas extending from the city center (Hand and Shepherd 2009; Haberlie et al. 2015), the U.S. Census Bureau (Mote et al. 2007; Walker et al. 2015), or Landsat-classified land cover datasets (Ashley et al. 2012). Recent work by Niyogi et al. (2017) suggests using a combined approach that considers both satellite-based imagery and population as human-induced activities can extend beyond a city core when defined strictly in terms of impervious surface. In this study, two methods of urban identification were used to create an urban boundary. The first method used the urban boundary coordinates from the U.S. Census Bureau (2010). The definition of an urban area consists of a spatially dense region of urban land use that contains greater than 50 000 people. The second method involved manually contouring an urban boundary from the urban/built-up categories from the 2011 NLCD dataset (Homer et al. 2015), which uses Landsat satellite data to classify land cover types. Both methods provided very similar latitudinal and longitudinal distances for the city (<5 km) and fundamentally did not alter the overall results of the study. Both city areas were compared with ambient population estimates from the 2012 LandScan dataset

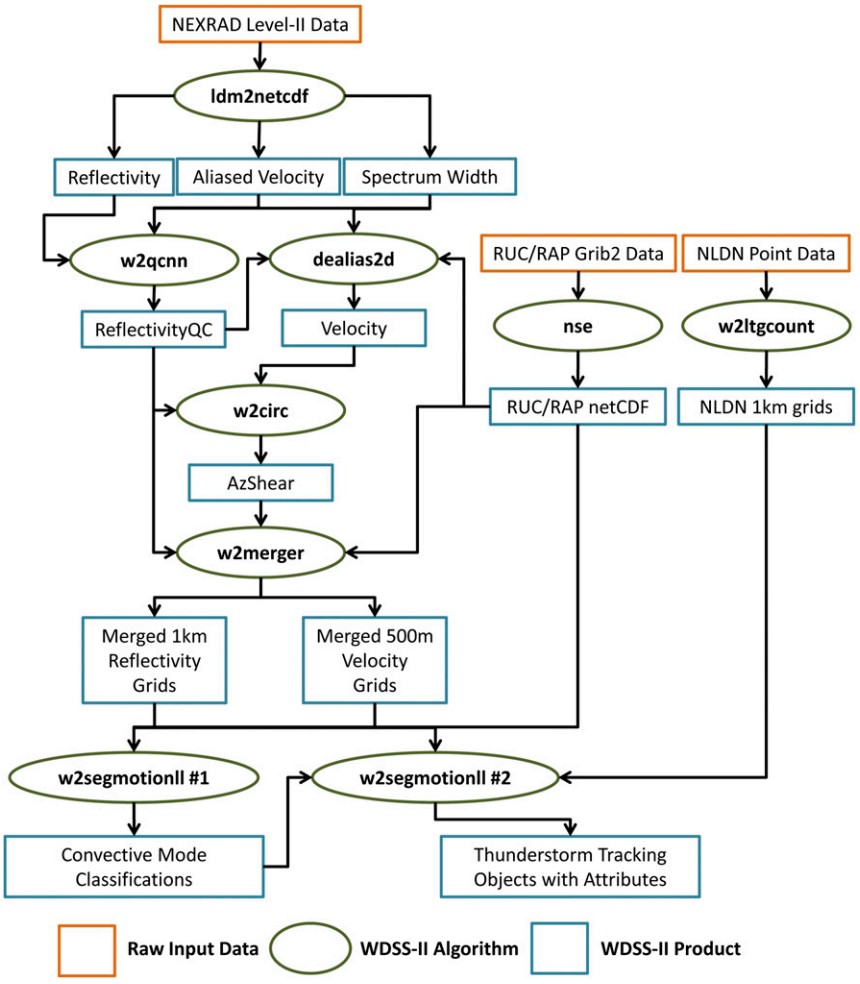

FIG. 3. Radar, model, and lightning processing workflow using WDSS-II.

(Bhaduri et al. 2007) to determine if the areas encapsulate the spatial distribution of population in the region. The city areas defined within this study contain 92%–96% of the ambient population when compared to the total population within a 25-km search radius surrounding each city. As a result, we consider these defined regions to be an adequate surrogate for both the physical components (i.e., buildings, impervious surface) and human components of a city (i.e., transportation).

4. Methods

a. Product generation and thunderstorm tracking

All radar, model, and lightning outputs were processed using the Warning Decision Support System–Integrated Information (WDSS-II; Lakshmanan et al. 2007b) software platform. The processing steps (flowchart in Fig. 3) for each of the products are described below.

1) CG LIGHTNING GRIDS

The CG strike location and time information from the NLDN dataset were binned into 1-min time steps and gridded onto a $0.01° \times 0.01°$ Cartesian grid (w2ltgcount; Fig. 3). To account for the increased detection efficiency of lower-amplitude events that may not actually be CGs (Cummins and Murphy 2009), all CGs with a peak amplitude $< |5|$ kA were excluded from the gridding process.

2) MODEL ANALYSIS GRIDS

Hourly model analysis data were ingested to reproject the basic meteorological fields (i.e., temperature, height, pressure, wind) at all vertical levels onto a common Cartesian grid. These fields served as inputs into the near-storm environment (nse; Fig. 3) algorithm to generate 2D convective instability fields, isothermal heights, and sounding profile products. These output fields were used to quality control the single-radar data [see

section 4a(3)] and generate several multiradar and tracking products [sections 4a(4) and 4a(5)].

3) SINGLE-RADAR PRODUCT GENERATION AND QUALITY CONTROL

Level-II radar data were ingested to generate the base products of reflectivity, aliased velocity, and spectrum width (ldm2netcdf; Fig. 3). Previous studies have mitigated the impact of nonmeteorological targets (e.g., birds/insects, ground clutter, electronic interference) and blockage by using a higher minimum reflectivity of 40 dBZ to identify a precipitation echo (Ashley et al. 2012; Haberlie et al. 2015). For this analysis, a neural network framework similar to that in Lakshmanan et al. (2007a) was used to identify and remove these sources of error while retaining lower reflectivity precipitation returns in a new ReflectivityQC field (w2qcnn; Fig. 3). ReflectivityQC was used in conjunction with the NWS operational dealiasing algorithm (Jing and Wiener 1993) to mitigate measurement errors in the radial projection of the environmental wind and generate a quality-controlled velocity field (dealias2d; Fig. 3). Both of these fields were inputs in the generation of single and vertically integrated azimuthal shear products (w2circ; Fig. 3) (Smith and Elmore 2004).

4) MULTIRADAR GRID GENERATION

The ReflectivityQC and vertically derived azimuthal shear from the individual radar sites along with the model data were inputs into an intelligent agent framework similar to that of Lakshmanan et al. (2006) to generate 3D Cartesian grids for reflectivity (azimuthal shear) at 0.01° latitude × 0.01° longitude (0.005° latitude × 0.005° longitude) spatial resolution and 1-min temporal resolution, across 33 vertical levels (w2merger; Fig. 3). These levels have 250-m vertical spacing from 0.5 to 3 km AGL, 500-m vertical spacing from 3 to 9 km AGL, and 1-km vertical spacing from 9 to 20 km AGL. To calculate VIL at a grid cell, the 3D reflectivity field was vertically interpolated using the Greene and Clark (1972) method. To exclude contamination from large ice or hail, interpolated reflectivity values exceeding 56 dBZ were capped at this value. MESH was calculated using the method of Witt et al. (1998) and uses both a vertical integration of reflectivity along with the locations of the 0° and −20°C isothermal heights to estimate the maximum diameter of a hailstone.

5) AUTOMATED THUNDERSTORM TRACKING

The storm identification and tracking algorithm in WDSS-II (w2segmotionll; Fig. 3) combines a watershed segmentation model (Lakshmanan et al. 2009) with K-means clustering (Bishop 2006) to identify thunderstorm objects based on a single observational variable (e.g., radar reflectivity). During the tracking process, summary statistics of other MRMS gridded attributes (e.g., maximum MESH, lightning count) can be calculated at each time step (Lakshmanan and Smith 2009). In this study, the algorithm was used to identify and track thunderstorm attributes in two stages. The first stage used composite reflectivity of 20 dBZ to identify and track storm objects (Hobson et al. 2012). Additionally, at this stage, the convective mode of each tracked storm was identified as either a supercell (Browning 1962) or nonsupercell through an automated analysis of the azimuthal shear fields. The storm classification and MRMS attributes were then reassigned to new storm objects through a second use of the w2segmotionll algorithm using reflectivity at the −10°C isothermal level with a minimum threshold of 20 dBZ. These new storm tracks were less susceptible to dramatic changes across time steps that can inadvertently break thunderstorm tracking (Herzog et al. 2014).

Quality control or hardware failures from a radar site can temporarily alter the magnitude and extent of a thunderstorm, causing a tracking algorithm to reclassify the storm as a new object and prematurely break an existing thunderstorm track. To assess the integrity of the thunderstorm tracks, a postevent track attachment technique [similar to that in Lakshmanan et al. (2015)] was used to validate that the end of tracking corresponded to the end of the storm's life cycle. The thunderstorm object boundaries were simplified using a convex hull (Devadoss and O'Rourke 2011), expanding this boundary by a radius of 5 km, and then projecting this new object forward along the mean direction of propagation for one more radar volume update interval (~5 min). If a new thunderstorm object appeared within the projected buffer, the object track of the original storm was extended. In the case of multiple new objects appearing in this search window, a selection was prioritized based on the 1) maximum storm lifetime, 2) closest start time, and 3) maximum spatial storm overlap within the search buffer.

b. Thunderstorm case selection

The information from the thunderstorm tracks was evaluated using two distinct methods. The first method examines how the maximum values of composite reflectivity, MESH, and VIL change by taking independent samples of thunderstorms upwind and downwind of each city. The second method examines the spatial distribution of the three radar fields within these two regions. Given the initial tracking process spans across all seasons, certain criteria were applied to define a thunderstorm event for analysis. First, a

thunderstorm object had to be tracked for at least 30 min to remove tracks that could be classified as noise or failed thunderstorms (Haberlie et al. 2015). Second, the object centroid (i.e., the geographic center of the object area) had to pass within the urban boundary. This removed many cases, where only a small fraction of a larger, more organized storm system was generally displaced from the city, from the dataset. Finally, the storm had to achieve a 35-dBZ composite reflectivity value and have one CG strike anywhere in its object area for at least one time step. Reflectivity thresholds ranging from 20 to 60 dBZ were examined and the 35-dBZ minimum coupled with the detection of lightning best removed events associated with nonconvective snow systems and stationary sources of noise that passed through radar quality control.

As noted in previous studies (e.g., Huff and Changnon 1972; Lowry 1998; Dixon and Mote 2003), examining thunderstorm days without any segmentation by season, synoptic regime, or diurnal limits could mask the effect urban areas have on thunderstorms. A subset of the data was created using seasonal, diurnal, and synoptic conditions with an increased likelihood of influence from urban effects. This ''urban favorable'' (hereafter referred to as UF) subset consisted of thunderstorm tracks that 1) occurred in the meteorological summer months (1 June–31 August) when the greatest urban–rural temperature differences are likely to occur (Gallo and Owen 1999); 2) initiated around the urban area in the midafternoon/evening hours (1800–0600 UTC), when the temperature difference and enhanced convective activity are most likely to occur (e.g., Mote et al. 2007; Haberlie et al. 2015); 3) occurred on days classified as moist tropical (MT) air masses [via the Spatial Synoptic Classification dataset of Sheridan (2002)] since these days yield greater UHI-induced precipitation events than dry airmass days (Dixon and Mote 2003; Hand and Shepherd 2009; Ashley et al. 2012); and 4) where <10% of the storm tracks were classified as a supercell (Hobson et al. 2012) to further remove days with increased vertical shear and meteorological forcing.

1) STORM-BASED MAXIMUM SAMPLING

As a result of the 1-min sampling interval on these thunderstorm objects, there is a degree of dependence between successive observations. Herzog et al. (2014) found the optimal decorrelation time scale is at least 9 min when sampling individual thunderstorm attributes (i.e., maximum reflectivity). At every time step, each thunderstorm object was categorized as either upwind (A), over the city (B), or downwind (C). For all objects meeting the above criteria, the maximum composite reflectivity, VIL, and MESH were sampled beginning at the 5-min time step and resampled every 10 min afterward. For instance, a storm lifetime of 30 min would be sampled at 5, 15, and 25 min, respectively. This initial 5-min time step (i.e., the average radar volume update time) was chosen to mitigate potentially sampling the initial or late stages of the thunderstorm.

Additionally, previous studies have shown that city size and orientation can affect the magnitude of the precipitation modification (Huff and Changnon 1973; Shepherd and Burian 2003; Schmid and Niyogi 2013). To account for this, a city-dependent search radius equal to the larger of the latitudinal or longitudinal distance was used to define the maximum distance a thunderstorm observation could be measured away from the urban footprint defined in section 3d. This equated to 127 km for DFW, 85 km for MSP, 56 km for OKC, and 47 km for OAX (Table 1). Other variations ranging to 50% and 150% of the city length or width were also investigated, but did not change the results. Comparisons in the distributions of upwind and downwind observations were evaluated using a two-sample Kolmogorov–Smirnov test (Wilks 1995).

2) SPATIAL DISTRIBUTION OF RADAR DATA

Hand and Shepherd (2009) noted the potential for variable magnitudes of precipitation modification to occur depending on the direction of the prevailing wind. To examine the spatial variation of thunderstorms, upwind and downwind regions were defined. Several past studies used isobaric wind fields (e.g., 700 hPa) from an observed sounding (Hand and Shepherd 2009; Haberlie et al. 2015) or model reanalysis fields (e.g., Burian and Shepherd 2005; Niyogi et al. 2017) for this purpose. In this study, with the unique availability of individually tracked storm objects, the upwind and downwind regions were defined on a storm-by-storm basis by using the mean direction of motion from the tracked thunderstorm object (Fig. 4).

Once defined, the maximum value of composite reflectivity, VIL, and MESH occurring at each grid cell was retained for the thunderstorm event. Complex shapes of urban sprawl are associated with each city; these result in an inconsistent start (end) to the upwind (downwind) region. To standardize these zones, each city was geometrically simplified using a convex hull operation, and the upwind and downwind regions were defined to begin 10 km away from this convex boundary. From the 10-km range onward, radar values were spatially binned in 1-km intervals and the amount of area covered in each bin was calculated (Fig. 4). From this information, the areal mean value of each parameter was calculated and tested for significance using a nonparametric two-sample permutation test of the mean (Wilks 1995).

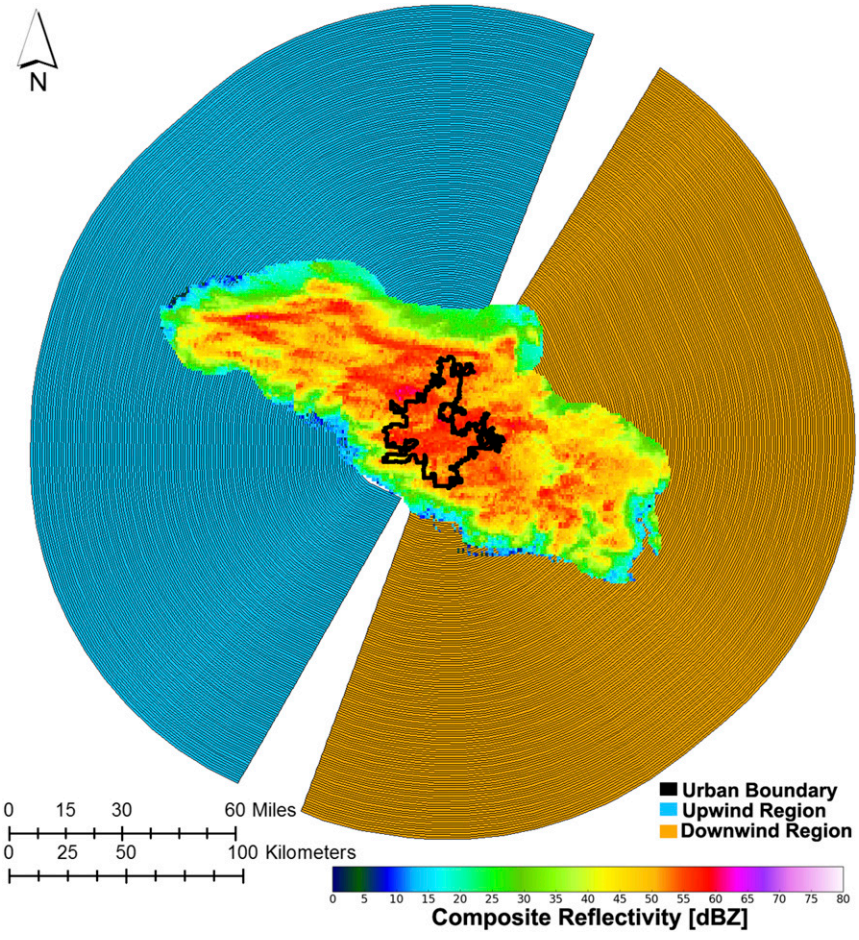

FIG. 4. Example of the upwind (blue) and downwind (orange) regions identified by the mean motion of a storm object interacting with OKC on 20 May 2011.

5. Results

a. Dataset overview

The number of storms analyzed was dependent on the city area, with 718 storms around DFW, 644 around MSP, 460 around OKC, and 391 around OAX (Fig. 5). At the northern latitudes, MSP and OAX had the highest percentage of thunderstorms occurring during the meteorological summer, accounting for 57% and 46% of all observations, respectively. DFW and OKC had the most thunderstorms during meteorological spring (1 March–31 May) with 41% and 38% of the respective storms. Summertime was the second-most active with 22% and 33%, respectively. Southern latitudes also had more storm occurrences in the fall and winter, accounting for 37% of storms in DFW, 29% in OKC, 26% in OAX, and 11% in MSP.

Grouping thunderstorm occurrence relative to city location revealed that each of the cities had the highest number of thunderstorm objects upwind and decaying over the city (AB). Storms that initiated over the city and moved downwind (BC) accounted for the second highest number. The smallest number of storms in our dataset were those that formed upwind of the city, tracked through the city, and then decayed downwind of the city (ABC). These tracks accounted for 10% of DFW storms, 18% of MSP storms, 30% of OKC storms, and 26% of OAX storms—negatively correlated to city size. The primary storm motion based on the centroid position for most events was from southwest to northeast in all cities, comparable to observations by Changnon and Huff (1961).

The UF subset accounts for 6% of DFW storms, 15% of MSP storms, 6% of OKC storms, and 7% of OAX storms. For DFW and MSP, a higher percentage of storms formed over the city (BC) than upwind (AB). Around OKC, there were 12 AB storms and 12 BC storms. OAX was the only city that continued to have more AB storms (11) than BC storms (9). Thunderstorm direction on these synoptically weak days was not as

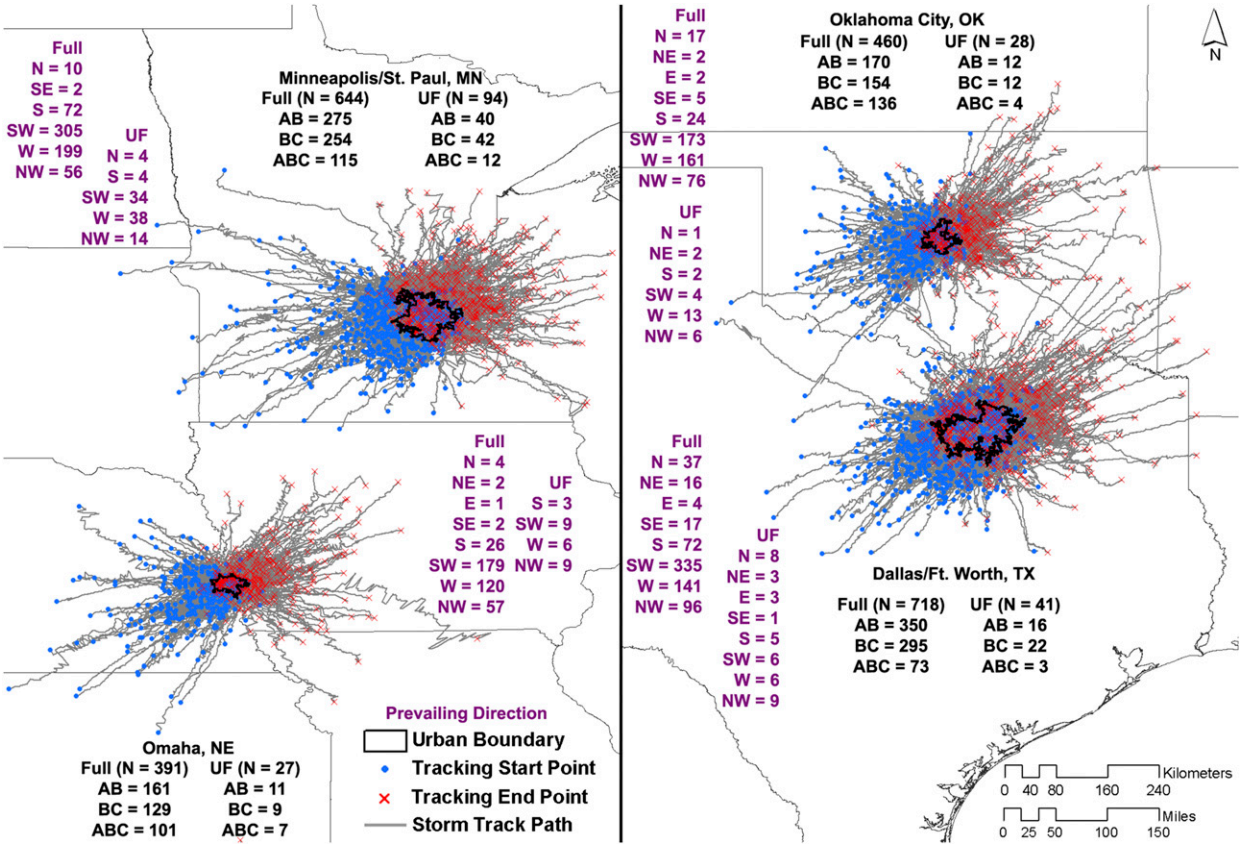

FIG. 5. Storm tracks identified using the criteria specified in section 4b. The total number of storms occurring around each city along with the number of storms that started upwind and ended over the city (AB), started over the city and ended downwind (BC), and crossed all three regions (ABC) are annotated in black for the full climatology and UF datasets. The prevailing directions of motion for thunderstorm objects from both datasets are annotated in purple.

uniform compared to tracks from the full dataset. 41% of DFW storms propagated from the north or northwest, MSP and OKC observed 40% and 46% of storms propagating from the west, and 66% of OAX storms moved from the northwest or southwest (Fig. 5).

b. Storm-sampling analysis

The maximum composite reflectivity (hereafter referred to as reflectivity; Fig. 6a), VIL (Fig. 6b), and MESH (Fig. 6c) for all days (solid lines) and the UF subset (dashed lines) revealed similar results across all cities in the full dataset but variable results in the UF subset. In the full dataset, there were more reflectivity and VIL samples from storms upwind of OAX and downwind of the other three cities (see number of samples N in Fig. 6). Additionally, all four cities had fewer MESH samples in the downwind region. In the UF subset, only DFW had a greater number of MESH observations downwind of the city area.

1) FULL DATASET

For DFW, the distributions of reflectivity, VIL, and MESH were significantly different ($p < 0.05$; left column in Fig. 6) between the upwind and downwind regions. There was a higher overall percentage and frequency of stronger storms in the upwind region. Around 98% (91%) of upwind (downwind) observations had a maximum reflectivity $\geq$ 40 dBZ [the minimum reflectivity threshold used to define a storm in Bentley et al. (2010), Ashley et al. (2012), and Haberlie et al. (2015)]. This trend continued at higher reflectivity thresholds; 53% (46%) of upwind (downwind) reflectivity samples exceeded 55 dBZ. Similar trends were also observed for multiple VIL and MESH thresholds.

Similar to observations around DFW, the upwind and downwind distributions of storm parameters for MSP were statistically significant ($p < 0.05$; Fig. 6, second column). There were a higher overall percentage and frequency of stronger storms in the upwind region. Around 97% (94%) of upwind (downwind) reflectivity samples

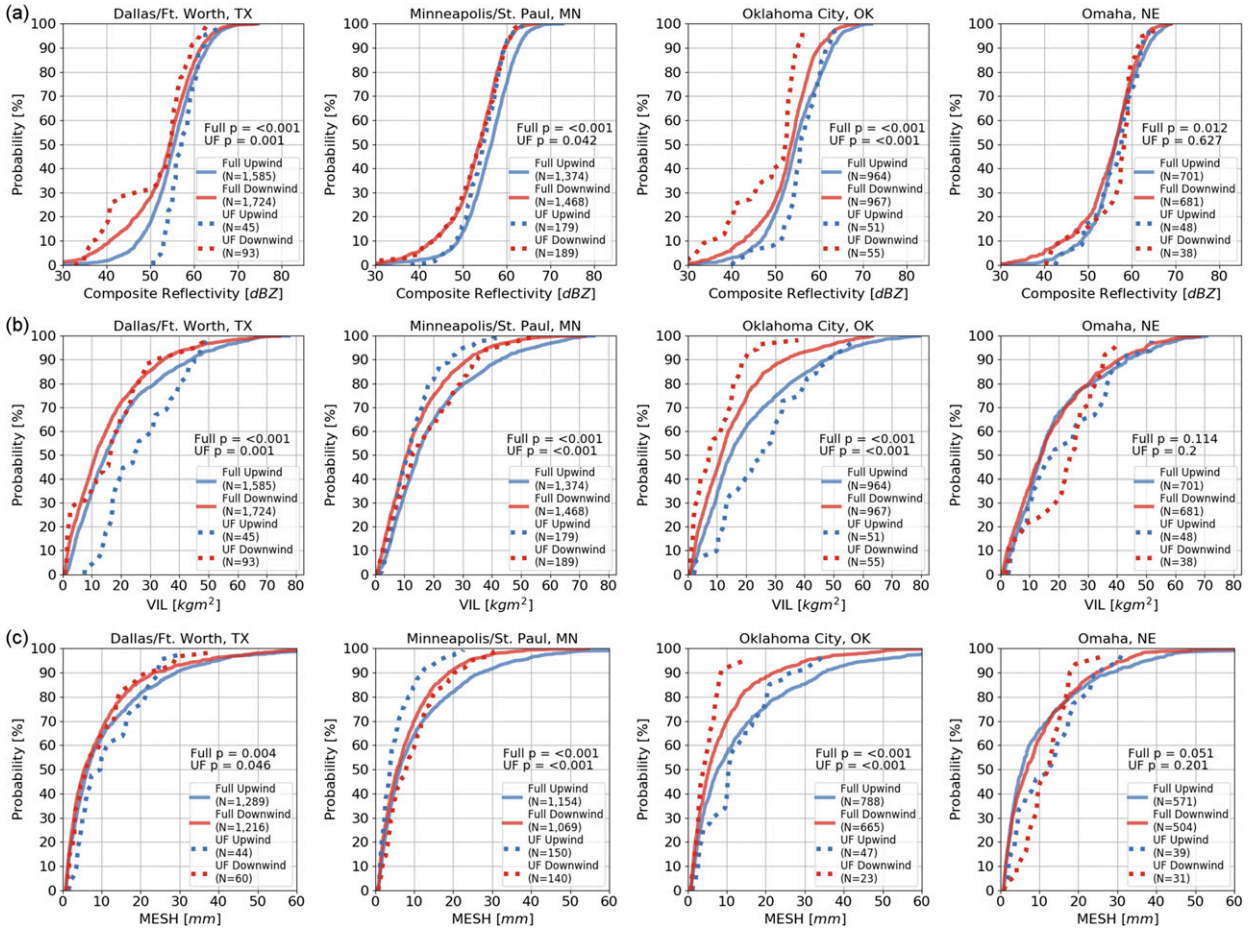

FIG. 6. CDF plots of (a) maximum reflectivity, (b) VIL, and (c) MESH upwind (blue) and downwind (red) of each city. The solid lines are distributions from the full climatology, and the dashed lines are distributions from the UF subset. The upwind and downwind distributions were compared for equality using a two-sample Kolmogorov–Smirnov test.

were greater than or equal to 40 dBZ. Comparable patterns were observed in both VIL and MESH with the median VIL around 14 kg m^{-2} (11 kg m^{-2}) and MESH around 6 mm (5 mm) in the upwind (downwind) region.

Near the OKC metro area, the numbers of reflectivity/VIL samples were similar in the upwind and downwind regions. However, there were a higher number of MESH samples in the upwind region and all distributions were statistically significant ($p < 0.05$; Fig. 6, third column). Similar to both DFW and MSP, around 97% (93%) and 47% (38%) of upwind (downwind) samples exceeded 40 and 55 dBZ, respectively. Similar patterns are observed throughout the entire range of VIL and MESH values.

OAX, because of its size, had the lowest number of storm samples when compared with other cities, with more in the upwind region for all three radar parameters (Fig. 6, right column). Similar to patterns for the other three cities, there were a greater number and overall percentage of maximum reflectivity samples in the upwind region for the entire range of reflectivity thresholds examined. The differences between the upwind and downwind distributions were statistically significant for only maximum reflectivity ($p < 0.05$), with substantial overlap occurring in both the MESH and VIL distributions.

2) UF SUBSET

Within the UF subset, the region downwind of DFW was more convectively active with more than 2 times the number of reflectivity/VIL samples and 36% more MESH samples. This provided a much larger range of values of all three radar parameters in the downwind region. This difference results in a lower percentage but higher total number of observations exceeding various thresholds of reflectivity and VIL in the downwind region. For example, all upwind ($N = 45$) and 82% of downwind ($N = 77$) samples had a maximum reflectivity exceeding 40 dBZ. The median VIL in the downwind

region is 16 kg m^{-2}, which was exceeded by 49 downwind samples compared to 35 in the upwind region. While there are more hail samples (MESH) downwind of DFW, nearly equal numbers of maximum MESH values were sampled between 5 and 15 mm. However, in cases of NWS-defined severe hail (≥25 mm or 1 in.), there were five observations that exceeded this criterion in the downwind region compared to one in the upwind region. This is likely due to the increased number of thunderstorm occurrences observed in the downwind region.

Around MSP, there were a greater number of reflectivity/VIL samples and, unlike DFW, fewer MESH samples in the downwind region. The differences in the upwind and downwind reflectivities were barely statistically significant ($p < 0.05$) with a similar frequency and percentage of samples exceeding 55 dBZ. When only examining storms within 50% of the city diameter (42 km instead of 84 km), the differences were no longer statistically significant ($p > 0.05$). For the two vertically derived products, MESH and VIL, there was a clear downwind enhancement in strength; both VIL and MESH had a greater number and percentage of downwind observations exceeding the thresholds of 8 kg m^{-2} and 2 mm, respectively.

The region downwind of OKC generally had a greater percentage and frequency of weaker reflectivity, MESH, and VIL values (Fig. 6, third column). Around 58% (10%) of upwind (downwind) samples had a maximum reflectivity ≥ 55 dBZ. No downwind occurrences of maximum VIL exceeded 38 kg m^{-2} while 24% upwind samples exceeded this threshold. There were fewer than half the number of MESH occurrences in the downwind region compared to the upwind region. Thirty-one percent of the upwind occurrences had a MESH greater than 16 mm while no occurrences were sampled in the downwind region.

Sampled thunderstorm occurrences around OAX had overlap at different radar thresholds for all three parameters (Fig. 6, right column). Furthermore, the upwind and downwind distributions were not statistically significantly different.

c. *Storm-based gridded climatology*

Analyses incorporating the gridded object area and accumulating the composite reflectivity (Fig. 7), VIL (Fig. 8), and MESH (Fig. 9) reveal common trends across all parameters in both datasets around DFW and MSP, and variable trends around OKC and OAX, dependent upon the parameter and distance from the city center. The gridded area and accumulations were calculated across variable upwind and downwind distances ranging from 50% to 150% of the maximum city diameter. Four ways of summarizing these data within each range interval upwind and downwind are shown in Figs. 7–9 and include the total number of thunderstorm objects at each range interval (panel a of each figure), the areal sum of the radar parameter (panel b), the overall area covered by the radar echo (panel c), and the areal mean value (panel d), which is the value in panel b divided by the value in panel c to give the mean value experienced at any given 1-km^2 grid cell.

1) FULL DATASET

Around DFW, the largest city examined, the upwind and downwind regions experienced a nearly equal number of thunderstorms from 10 to 64 km (i.e., 50% city diameter) (Fig. 7a). Yet, the total reflectivity in the downwind region (Fig. 7b) was around 9% higher over a 10% larger area (Fig. 7c). This resulted in a lower areal mean reflectivity (Fig. 7d) in the downwind region. A similar pattern was seen in the VIL (Figs. 8a–d, left column), with a 2%–4% increase in cumulative VIL occurring over a 10%–21% larger area. This larger spatial spread of VIL values over a larger area in the downwind region lowered the areal mean VIL. Unlike VIL, MESH values were not available at every pixel, particularly if there was no reflectivity measured at temperatures < 0°C. This limited the number of samples of "hail producing" thunderstorms. All ranges downwind of DFW had a lower cumulative MESH (from −1% to −5%) occurring over a much larger area (15%–18%) compared to observations in the upwind region, resulting in a much lower areal mean MESH in the downwind region.

MSP experienced 10% more downwind thunderstorms out to 43 km (50% city diameter) and 15% more thunderstorms out to 128 km (150% city diameter) (Fig. 7a). Like DFW, however, the areal mean reflectivity was lower in the downwind region (~40 dBZ km^{-2}) at all ranges compared to the upwind region (~42 dBZ km^{-2}) (Fig. 7d) as a result of the larger areal coverage of lower-reflectivity values in the downwind region. A similar pattern was observed with the VIL parameter. Cumulative MESH was 12%–35% lower in the downwind region (Fig. 9b) and occurred over a 5%–19% smaller area (Fig. 9c). The weaker MESH values over a smaller area resulted in a lower areal mean MESH measured at all downwind ranges compared to the upwind region (Fig. 9d).

From 10 to 28 km (50% city diameter) downwind of OKC, there were a lower number of storm occurrences. They consisted of weaker cumulative reflectivity over a smaller spatial area in the downwind region. From 10 to 84 km (150% city diameter), an opposite pattern emerged, with a higher cumulative reflectivity over a larger area (Figs. 7a–c). At all ranges, however, the areal

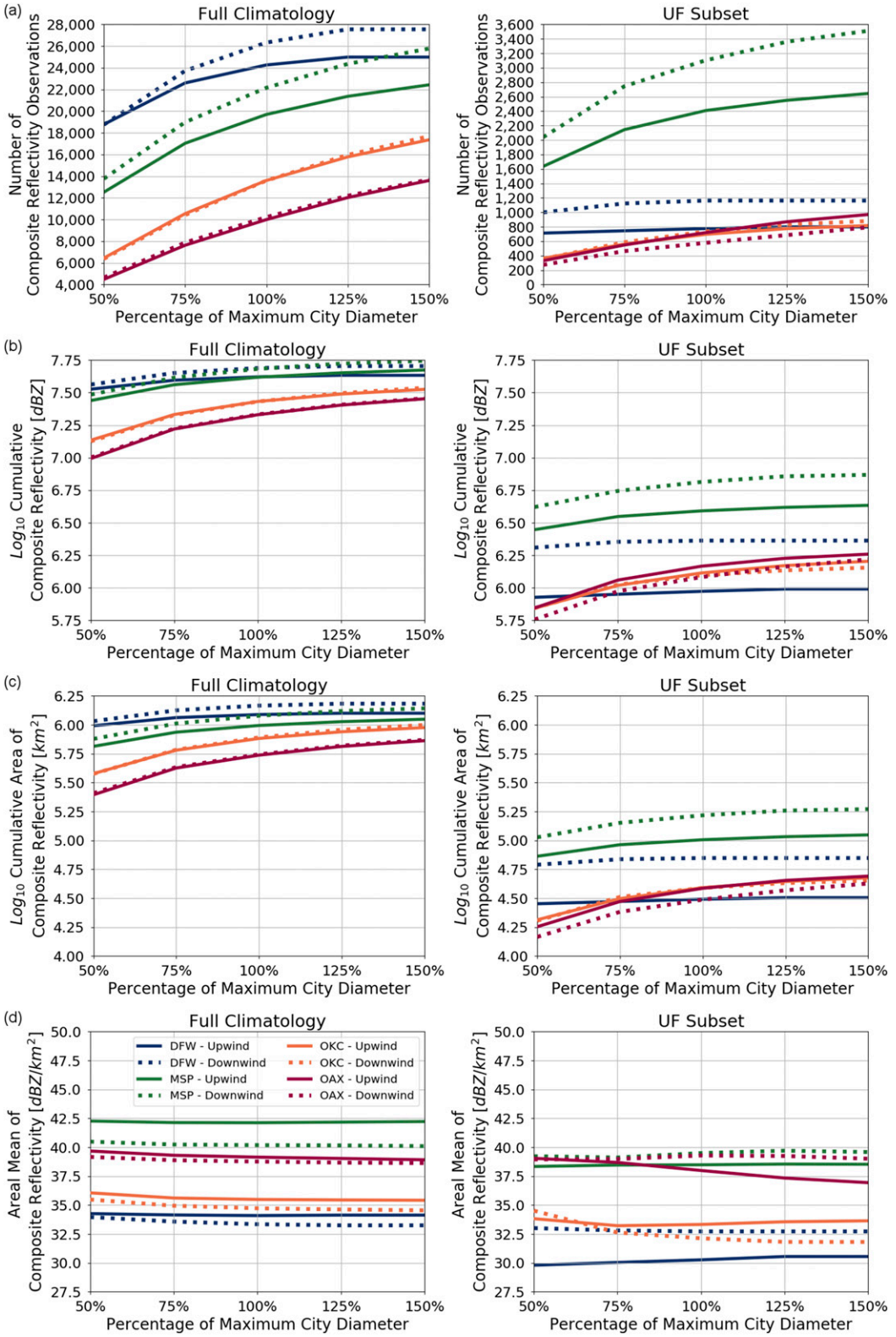

FIG. 7. Values of composite reflectivity for the (left) full climatology and (right) UF subset at ranges upwind (solid line) and downwind (dashed line) 50%–150% times the maximum city diameter. These regions are summarized by (a) the number of thunderstorm objects, (b) the cumulative reflectivity, (c) the cumulative area affected, and (d) the areal mean composite reflectivity.

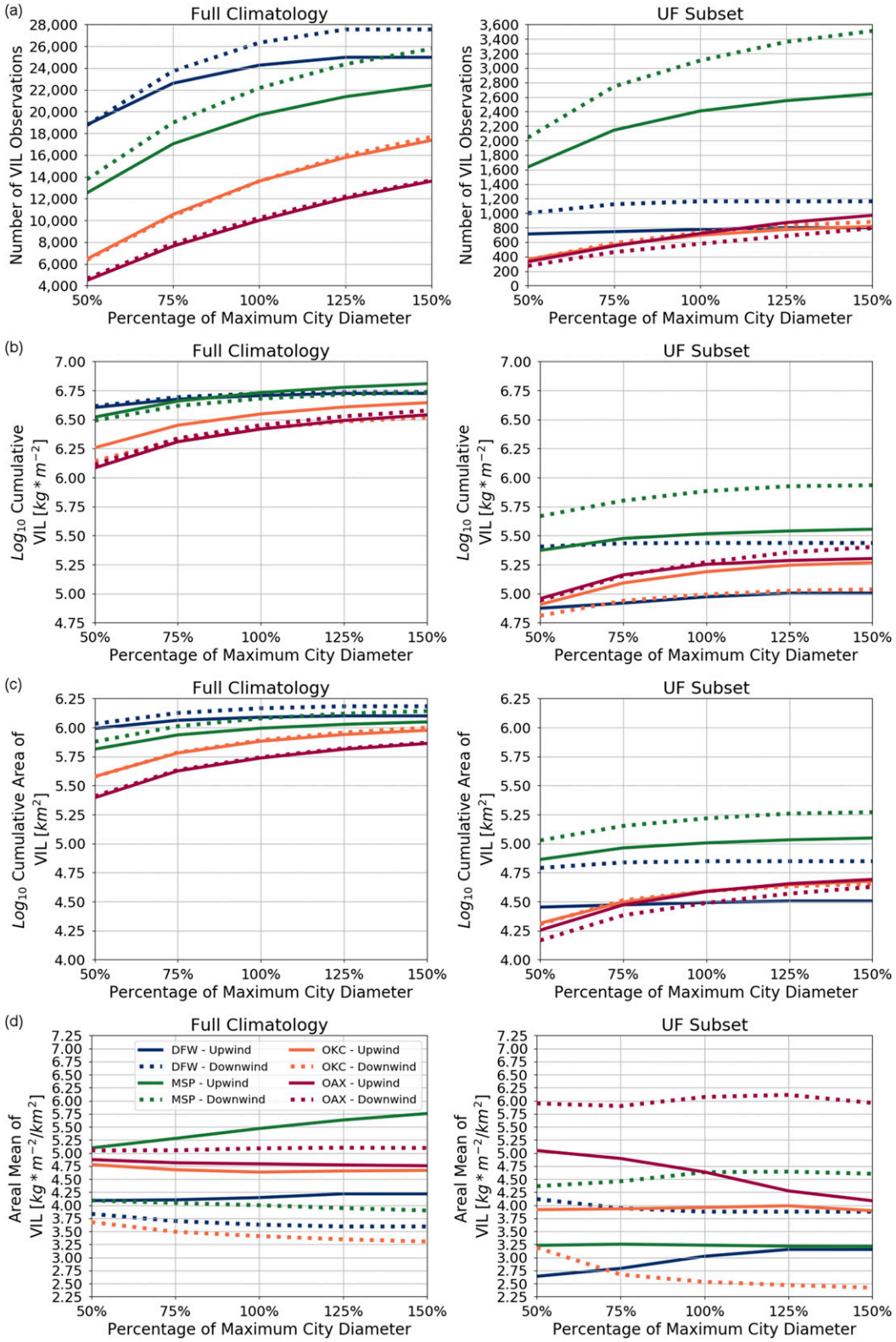

FIG. 8. As in Fig. 7, but for VIL.

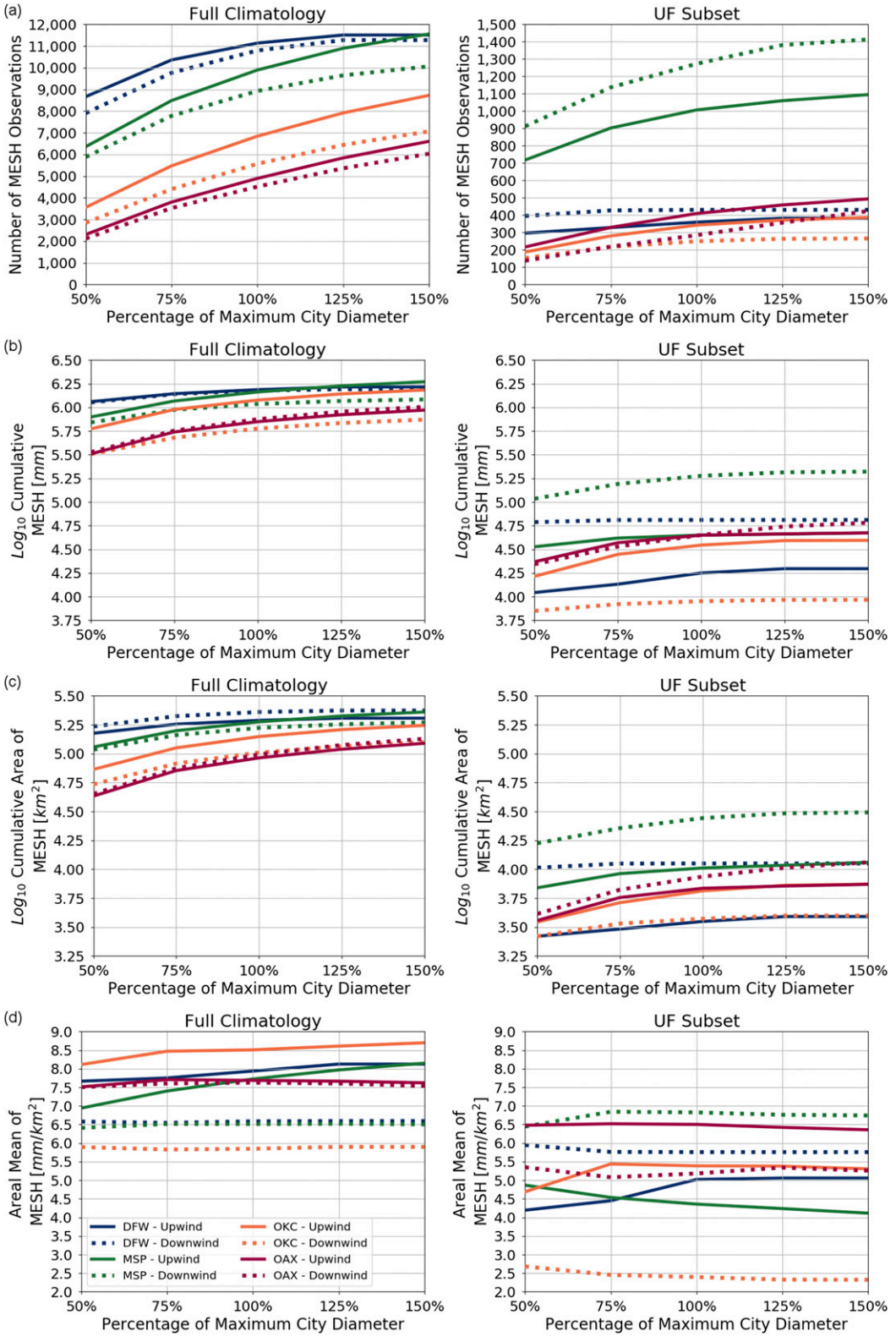

FIG. 9. As in Fig. 7, but for MESH.

mean reflectivity was lower in the downwind region compared to the upwind region (Fig. 7d). The cumulative VIL value downwind of OKC was about 24% lower than the upwind region, leading to a much lower areal mean VIL in this region at all ranges (Fig. 8d). Cumulative MESH was also around 50% lower in the downwind region, with the MESH signatures covering a 27% smaller spatial area (Figs. 9b,c). These weak and sparse MESH tracks downwind of OKC not surprisingly resulted in a lower areal mean MESH, about 3 mm km^{-2} lower than in the upwind region (Fig. 9d).

Like MSP, OAX has a higher number of reflectivity grid cells (Fig. 7a) and cumulative reflectivity (Fig. 7b), occurring over a wider area (Fig. 7c). This resulted in a lower areal mean reflectivity (Fig. 7d) in the downwind region. OAX was the only area to have a higher areal mean VIL in the downwind region within the full dataset, with a 7%–9% increase in cumulative VIL over only a 2%–3% increase in area. This was not observed with the MESH parameter; a higher cumulative MESH (Fig. 9b) measured over a larger area (Fig. 9c) resulted in a lower areal mean MESH (Fig. 9d).

2) UF SUBSET

Unlike the trends observed in the full dataset, the area downwind of DFW had up to 51% more thunderstorm observations (Fig. 7a, right column), resulting in a 153% increase in cumulative reflectivity (Fig. 7b) and occurring over up to a 131% larger area (Fig. 7c) in the UF subset. As a result, the areal mean reflectivity was about 3 dBZ km^{-2} higher in the downwind region on UF days. Similar patterns in VIL were seen around DFW. The cumulative VIL (areal coverage) was 239% (132%) higher in the downwind region, yielding an increased areal mean VIL downwind of DFW on UF days (Figs. 8b–d). There were also a greater number of MESH observations downwind of DFW, with up to a 455% increase in cumulative MESH (Fig. 9b) over a 291.6% larger area (Fig. 9c). This resulted in a higher areal mean MESH in the downwind region (Fig. 9d). At ranges beyond 127 km from DFW, the difference in areal mean MESH was not statistically significant ($p > 0.05$) and was the only occurrence of such a result out of all of the areal mean comparisons for each city, radar parameter, and case dataset.

Similar to DFW, the area downwind of MSP had up to 33% more thunderstorm observations (Fig. 7a) and up to a 132% (68%) increase in cumulative reflectivity (areal coverage) (Figs. 7b,c). This resulted in an elevated downwind areal mean reflectivity at all ranges examined (Fig. 7d). Cumulative VIL (areal coverage) values were 143% (68%) higher in the downwind region compared to the upwind region and, thus, had a higher downwind areal mean VIL at all ranges from MSP. Trends in MESH values were similar to those observed for VIL with a higher areal mean MESH observed in the area downwind of MSP.

OKC showed a 2% decline in the number of downwind storms out to 28 km (50% city diameter); however, the downwind cumulative reflectivity was <1 % higher and covered an area 2% smaller than the upwind region, resulting in a slightly higher areal mean reflectivity in the downwind region. Yet, the upwind region encompassing ranges > 42 km away from OKC experienced larger, stronger storms (Figs. 7b,c) than the downwind area of equal distance, even in the UF subset. This produced lower areal mean reflectivity values in the downwind region (Fig. 7d). Cumulative VIL values were 41% lower in the downwind region out to 84 km (150% city diameter) and encompassed an area around 6% smaller than the upwind region (Figs. 8b,c). This resulted in a lower areal mean VIL in the downwind region, the opposite of the VIL patterns around DFW and MSP (Fig. 8d). Areas downwind of OKC had fewer MESH-producing thunderstorm occurrences; as such, this area had a lower cumulative MESH that covered a smaller area (Figs. 9a–c). This resulted in mean MESH values at least 2 mm smaller in the downwind region (Fig. 9d).

At all range intervals downwind of OAX in the UF subset, there were fewer thunderstorm occurrences in the downwind region, and there was a 9%–19% decline in cumulative reflectivity (Fig. 7b) over a 14%–20% smaller area (Fig. 7c). From 10 to 28 km (50% city diameter), the percentage decline in cumulative reflectivity was slightly lower than the percentage decline in the affected area for both the upwind and downwind regions, producing nearly equal mean areal reflectivity for both regions. At subsequent ranges from OAX, there was a higher areal mean reflectivity in the downwind region (Fig. 7d). Both the number of thunderstorm occurrences and the total affected area were lower in the downwind region at all ranges surrounding OAX. However, cumulative VIL was higher when grid cells beyond 47 km in the downwind region were included (Figs. 8a–c). As a result, areal mean VIL values downwind of OAX were 18%–46% higher in the downwind region and comparable to observations from the full dataset (Fig. 8d). Similar to OKC, areas downwind of OAX had a lower number of MESH-producing thunderstorm occurrences (Fig. 9a). However, the areal coverage of MESH in this region was much larger, covering 14%–55% more area than the upwind region. Cumulative MESH values also were higher from 47 km (100% city diameter) and beyond, but not large enough to compensate for the increases in overall areal coverage

(Figs. 9b,c). Thus, the mean MESH was lower at all downwind ranges evaluated (Fig. 9d).

6. Discussion

This study incorporated the techniques from the MRMS and WDSS-II frameworks to process radar, lightning, and near-storm environmental fields in order to create over 2.6 million grids of reflectivity, MESH, and VIL at a very high spatial (≤1 km) and temporal (1 min) resolution. The methods employed in this study address two main assumptions used in prior urban thunderstorm studies using fixed observational gauges (Huff and Changnon 1972; Jauregui and Romales 1996; Diem and Mote 2005; Niyogi et al. 2017) and remote sensing systems (Shepherd et al. 2002; Dixon and Mote 2003; Mote et al. 2007; Hand and Shepherd 2009; Bentley et al. 2010; Niyogi et al. 2011).

First, many of these studies cannot quantify the number of storms that directly interacted with a city. For instance, Mote et al. (2007) examined hourly precipitation patterns near Atlanta and observed instances where precipitation downwind of Atlanta was actually initiated in the mountains and not directly due to urban influences. Through the use of an automated storm tracking system, it can be captured exactly where and when a thunderstorm interacted with an urban area. Second, prevailing wind has predominantly been estimated in past studies through use of NWS radiosonde observations (Hand and Shepherd 2009; Haberlie et al. 2015) or isobaric pressure levels from model reanalysis data (e.g., Burian and Shepherd 2005; Niyogi et al. 2017). As noted in Niyogi et al. (2017), the 850-hPa wind field was used to assess the boundary layer winds, but individual storm cells can deviate from this flow. Within this study, the 1-min thunderstorm track defined the upwind and downwind regions on an individual storm basis. Furthermore, these upwind and downwind regions were standardized by the relative position from the city, allowing for the calculation of bulk statistics independent of geographic location, instead of focusing on a predefined region based on a monthly or seasonal average of flow (i.e., 25–75 km east of DFW).

Nonetheless, our analyses are not free from limitations. Thunderstorms do not always follow an ordinary life cycle (i.e., growth, maturity, decay) without being subject to interactions such as splitting and merging (Lakshmanan et al. 2009). While these features can be documented by smaller-scale and often time-consuming manual analyses of thunderstorms (e.g., Niyogi et al. 2011), it is assumed these impacts were minimized in this study. Furthermore, the way WSR-88D data are collected and calibrated is dependent on the radar hardware and volume coverage pattern chosen by the radar operator. While the blending of multiple radars, through the use of a system like MRMS, provided increased volumetric coverage of a thunderstorm over single-radar studies (Maddox et al. 1999; Lakshmanan et al. 2006; Smith et al. 2016), all studies using WSR-88D data are limited by how these data are collected (e.g., volumetric scanning strategies, etc.) and calibrated. Signal calibration continues to be a challenge for any analysis using radar, particularly when comparing signals from separate radar systems (Atlas 2002). The WSR-88D network is not immune from these potential sources of error; yet, routine checking and automatic monitoring procedures are in place to minimize the length of time these errors persist (Serafin and Wilson 2000). The criteria that each thunderstorm object's centroid pass through the urban area and be tracked for at least 30 min ensured urban interaction and allowed radar attributes to be independently sampled at least three times per thunderstorm. Lowering this tracking threshold to 10 min only increased the number of total cases by 7% around all cities. Regardless, thunderstorms with shorter lifetimes or thunderstorms that form downwind of the city as a result of the role of potential urban-induced convergent zones (e.g., Bornstein and Lin 2000) or aerosol entrainment (e.g., Schmid and Niyogi 2017) were not included in this study but warrant future attention.

Both analysis methods, particularly the spatial gridding method, revealed stronger reflectivity and vertically integrated quantities downwind of DFW (~4600 km^2) and MSP (~2650 km^2), the two larger cities in this study. Additionally, this was most evident on UF days compared to the full dataset. For both of these cities, a higher number of thunderstorms developed over the city and propagated downwind on these days, similar to the results of Haberlie et al. (2015) around Atlanta. This pattern would imply that larger cities, with a widespread distribution of impervious surface materials, allow for greater anthropogenic influences (e.g., pollution) and could generate new and strengthen existing thunderstorms at a greater magnitude downwind than small cities given the appropriate conditions.

Around OKC, a city 40% the size of MSP, an increase in downwind areal mean reflectivity did occur when examining an area from 10 to 28 km, but not at further downwind ranges. Areal means of MESH and VIL as well as independent samples of the maximum reflectivity, MESH, and VIL tended to be higher in the upwind region around OKC on UF days. Hand and Shepherd (2009) identify the north-northeast region downwind of OKC to be the climatologically wettest region; however, this region only aligns with 6 of the 28 thunderstorms

objects evaluated in our UF subset and limits any sort of comparison herein. Regardless, any downwind enhancement in these radar parameters is not observed in the thunderstorms for OKC, as was noted for DFW and MSP.

Around OAX, with an urban footprint that is 26% the size of MSP, there was no statistically significant difference between the upwind and downwind samples of maximum reflectivity, VIL, and MESH in the UF subset. Furthermore, unlike what was observed around DFW or MSP, there was no immediate downwind enhancement in areal mean reflectivity or MESH on UF days. This, coupled with being the smallest city in the study, introduces some uncertainty as to how much the urban area of OAX can augment thunderstorms. Other geographically collocated factors, such as the relatively homogeneous amount of cultivated crops surrounding this urban area, are known to have a definitive impact. Clark and Arnitt (1995) found that surfaces with moist soil and vegetation cover were most conducive to convective development. Gero and Pitman (2006) observed through numerical model simulations that the replacement of agricultural land with shrubland hindered storm development upwind from Sydney, Australia. Additional numerical modeling and observational studies are needed to delineate the role of homogeneous versus heterogeneous land cover on storm initiation comparable to studies of the effects of topography (e.g., Lowry 1998; Niyogi et al. 2006).

DFW ($\sim$4600 km^2) and MSP ($\sim$2650 km^2) both showed a downwind enhancement in composite reflectivity, MESH, and VIL from both analysis methods on UF days compared to OKC ($\sim$1060 km^2) and OAX ($\sim$700 km^2). This indicates the contributing role of city size in precipitation modification. Schmid and Niyogi (2013) modeled the effects of city size and found that both the maximum average heat island and the amount of precipitation modification increased linearly with city radii ranging from 5 to 20 km with fairly constant effects observed beyond this threshold. While a definitive size threshold cannot be defined here, size is only one factor contributing to the magnitude of urban modification. Other contributing factors such as the regional climate (Roth 2007), the variable influence of urban-induced aerosols on precipitation timing and magnitude (Rosenfeld et al. 2008; Lebo 2014; Schmid and Niyogi 2017), the surrounding regional landscape species variability (Rabin et al. 1990), and soil moisture gradients as a result of natural and irrigation practices (Barnston and Schickedanz 1984; Niyogi et al. 2006; DeAngelis et al. 2010), coupled with urban size/shape, could provide a geographically dependent alteration to the extent of precipitation modification.

7. Conclusions

This study highlights the utility of the MRMS framework to blend multi-instrument datasets, identify thunderstorm areas, and track storm attributes. Five years' worth of composite reflectivity, MESH, and VIL grids were created and examined for four cities of varying sizes (DFW, MSP, OKC, and OAX) to better understand how city size affects thunderstorms. Overall, city size seems to be a contributing factor in enhancing the coverage and magnitude of these radar variables in the downwind region; however, these effects were not as clearly observed when examining objects across all seasons and synoptic regimes. Sampling each thunderstorm object every 10 min reveals that a greater overall percentage and frequency of thunderstorms had a higher composite reflectivity, MESH, and VIL occurring upwind of all four cities. Spatially accumulating these fields revealed a higher areal mean of all three parameters occurring upwind of all four cities, with the exception of VIL around OAX.

Taking a subset of thunderstorms and matching historical seasonal, temporal, and synoptic environments where urban modification is likely reveals an increased number of thunderstorms forming and moving downwind of DFW and MSP, the two largest cities examined. This resulted in higher areal mean values of composite reflectivity, MESH, and VIL at several ranges downwind of both cities compared to the upwind region. This pattern was not observed in all radar fields downwind of OKC and OAX, cities roughly 40% and 26% the size of MSP, particularly in analyses of the vertically derived fields of MESH and VIL. This could be indicative of a lack of influence of small to midsized urban areas ($\leq\sim$1100 km^2 based on our city selection). Yet, this subset reveals that areas downwind of larger cities are susceptible to more frequent and stronger thunderstorms that are likely initiated by the urban environment and are subject to the occurrence of heavier rainfall and increased hail potential.

The thresholds used to delineate UF environments resulted in an 84%–94% reduction in the number of thunderstorm cases based on observations of thunderstorms measured in prior studies (Dixon and Mote 2003; Mote et al. 2007; Haberlie et al. 2015). The contrast between the full dataset and the UF subset reveals that the percentage of storms capable of being modified over a city due to seasonal, temporal, and synoptic influences is a small fraction of the number of storms that affect cities on a yearly basis. Based on the percentage of UF storms retained from the full dataset, MSP (15%) compared to DFW (6%), OKC (6%), and OAX (7%) has the highest potential for the urban domain to influence storm structure and intensity. However, the inconsistent nature of

these precipitation modification patterns through the lens of the full climatology of all cities raises the question as to whether the statistical predictability of these patterns is achievable, since instantaneous measures of other suspected modification variables (e.g., spatial aerosol loading; Van den Heever and Cotton 2007; Kawecki et al. 2016) may not be readily observable.

For future retrospective analyses of thunderstorms, we promote the use of the MRMS system because of its ability to blend information from multiple sources onto a common grid. Since the completion of this study, there have been improvements in both the data quality and longevity of archived data available over the United States. The recent upgrade of the WSR-88D network with polarimetric capability provides additional information on the hydrometeor distributions of convective systems (e.g., Zrnić and Ryzhkov 1999). Furthermore, the launch of the Geostationary Operational Environmental Satellite-R series satellite with the Advanced Baseline Imager (Schmit et al. 2017) and Geostationary Lightning Mapper (Goodman et al. 2013) instruments provides significant spatiotemporal improvements in the observation and monitoring of both surface-based and atmospheric phenomena that hindered prior satellite analyses of thunderstorms (e.g., Cintineo et al. 2013). These new datasets are open for exploration with the MRMS system and could provide the next set of observational evidence to diagnose the role urban areas have on influencing thunderstorm evolution.

Acknowledgments. The authors thank Gregory Dean and Kiel Ortega for their assistance in downloading the large volume of radar data for this study. We also thank Bethany Hardzinski, Paul Downes, Jonathon King, and Benjamin Herzog for their assistance with initial data collection and algorithm evaluation. We acknowledge useful discussions with Kevin Manross on the methods of this paper. We would finally like to thank Dev Niyogi and two anonymous reviewers, whose comments and philosophical questions improved the content of this manuscript. This work was funded through the NASA Interdisciplinary Science Program Project (NNX12AM89G) as part of the grant "Storms, Forms, and Complexity of the Urban Canopy: How Land Use, Settlement Patterns, and the Shapes of Cities Influence Severe Weather."

REFERENCES

Angel, S., J. Parent, D. L. Civco, A. Blei, and D. Potere, 2011: The dimensions of global urban expansion: Estimates and projections for all countries, 2000–2050. *Prog. Plann.*, **75**, 53–107, https://doi.org/10.1016/j.progress.2011.04.001.

Ashley, W. S., M. L. Bentley, and J. A. Stallins, 2012: Urban-induced thunderstorm modification in the southeast United States. *Climatic Change*, **113**, 481–498, https://doi.org/10.1007/s10584-011-0324-1.

Atkinson, B. W., 1971: The effect of an urban area on the precipitation from a moving thunderstorm. *J. Appl. Meteor.*, **10**, 47–55, https://doi.org/10.1175/1520-0450(1971)010<0047:TEOAUA>2.0.CO;2.

Atlas, D., 2002: Radar calibration: Some simple approaches. *Bull. Amer. Meteor. Soc.*, **83**, 1313–1316, https://doi.org/10.1175/1520-0477(2002)083<1313:RCSSA>2.3.CO;2.

Barnston, A. G., and P. T. Schickedanz, 1984: The effect of irrigation on warm season precipitation in the southern Great Plains. *J. Climate Appl. Meteor.*, **23**, 865–888, https://doi.org/10.1175/1520-0450(1984)023<0865:TEOIOW>2.0.CO;2.

Benjamin, S. G., and Coauthors, 2004: An hourly assimilation–forecast cycle: The RUC. *Mon. Wea. Rev.*, **132**, 495–518, https://doi.org/10.1175/1520-0493(2004)132<0495:AHACTR>2.0.CO;2.

——, and Coauthors, 2016: A North American hourly assimilation and model forecast cycle: The Rapid Refresh. *Mon. Wea. Rev.*, **144**, 1669–1694, https://doi.org/10.1175/MWR-D-15-0242.1.

Bentley, M. L., W. S. Ashley, and J. A. Stallins, 2010: Climatological radar delineation of urban convection for Atlanta, Georgia. *Int. J. Climatol.*, **30**, 1589–1594, https://doi.org/10.1002/joc.2020.

Bhaduri, B., E. Bright, P. Coleman, and M. Urban, 2007: LandScan USA: A high resolution geospatial and temporal modeling approach for population distribution and dynamics. *GeoJournal*, **69**, 103–117, https://doi.org/10.1007/s10708-007-9105-9.

Bishop, C. M., 2006: *Pattern Recognition and Machine Learning.* Springer Science, 738 pp.

Bornstein, R. D., and M. LeRoy, 1990: Urban barrier effects on convective and frontal thunderstorms. *Extended Abstracts, Fourth Conf. on Mesoscale Processes*, Boulder, CO, Amer. Meteor. Soc., 120–121.

——, and Q. Lin, 2000: Urban heat islands and summertime convective thunderstorms in Atlanta: Three case studies. *Atmos. Environ.*, **34**, 507–516, https://doi.org/10.1016/S1352-2310(99)00374-X.

Boussaton, M. P., S. Soula, and S. Coquillat, 2007: Total lightning activity in thunderstorms over Paris. *Atmos. Res.*, **84**, 221–232, https://doi.org/10.1016/j.atmosres.2006.07.003.

Brooks, H. E., C. A. Doswell III, and M. P. Kay, 2003: Climatological estimates of local daily tornado probability for the United States. *Wea. Forecasting*, **18**, 626–640, https://doi.org/10.1175/1520-0434(2003)018<0626:CEOLDT>2.0.CO;2.

Brown, R. A., V. T. Wood, and D. Sirmans, 2002: Improved tornado detection using simulated and actual WSR-88D data with enhanced resolution. *J. Atmos. Oceanic Technol.*, **19**, 1759–1771, https://doi.org/10.1175/1520-0426(2002)019<1759:ITDUSA>2.0.CO;2.

——, B. A. Flickinger, E. Forren, D. M. Schultz, D. Sirmans, P. L. Spencer, V. T. Wood, and C. L. Ziegler, 2005: Improved detection of severe storms using experimental fine-resolution WSR-88D measurements. *Wea. Forecasting*, **20**, 3–14, https://doi.org/10.1175/WAF-832.1.

Browning, K. A., 1962: Cellular structure of convective storms. *Meteor. Mag.*, **91**, 341–350.

Burian, S. J., and J. M. Shepherd, 2005: Effects of urbanization on the diurnal rainfall pattern in Houston. *Hydrol. Processes*, **19**, 1089–1103, https://doi.org/10.1002/hyp.5647.

Changnon, S. A., Jr., 1968: The La Porte weather anomaly—Fact or fiction? *Bull. Amer. Meteor. Soc.*, **49**, 4–11.

——, 1979: Rainfall changes in summer caused by St. Louis. *Science*, **205**, 402–404, https://doi.org/10.1126/science.205.4404.402.

——, 1980: More on the La Porte anomaly: A review. *Bull. Amer. Meteor. Soc.*, **61**, 702–711, https://doi.org/10.1175/1520-0477(1980)061<0702:MOTLPA>2.0.CO;2.

——, and F. A. Huff, 1961: Studies of radar-depicted precipitation lines. Illinois State Water Survey Sci. Rep. 2, Urbana, IL, 63 pp., http://hdl.handle.net/2142/55400.

——, ——, and R. G. Semonin, 1971: METROMEX: An investigation of inadvertent weather modification. *Bull. Amer. Meteor. Soc.*, **52**, 958–967, https://doi.org/10.1175/1520-0477(1971)052<0958:MAIOIW>2.0.CO;2.

——, R. T. Shealy, and R. W. Scott, 1991: Precipitation changes in the fall, winter, and spring caused by St. Louis. *J. Appl. Meteor.*, **30**, 126–134, https://doi.org/10.1175/1520-0450(1991)030<0126:PCIFWA>2.0.CO;2.

Chronis, T., L. D. Carey, C. J. Schultz, E. V. Schultz, K. M. Calhoun, and S. J. Goodman, 2015: Exploring lightning jump characteristics. *Wea. Forecasting*, **30**, 23–37, https://doi.org/10.1175/WAF-D-14-00064.1.

Cintineo, J. L., T. M. Smith, V. Lakshmanan, H. E. Brooks, and K. L. Ortega, 2012: An objective high-resolution hail climatology of the contiguous United States. *Wea. Forecasting*, **27**, 1235–1248, https://doi.org/10.1175/WAF-D-11-00151.1.

——, M. J. Pavolonis, J. M. Sieglaff, and A. K. Heidinger, 2013: Evolution of severe and nonsevere convection inferred from GOES-derived cloud properties. *J. Appl. Meteor. Climatol.*, **52**, 2009–2023, https://doi.org/10.1175/JAMC-D-12-0330.1.

——, ——, ——, and D. T. Lindsey, 2014: An empirical model for assessing the severe weather potential of developing convection. *Wea. Forecasting*, **29**, 639–653, https://doi.org/10.1175/WAF-D-13-00113.1.

Clark, C. A., and R. W. Arnitt, 1995: Numerical simulation of the effect of soil moisture and vegetation cover on the development of deep convection. *J. Appl. Meteor.*, **34**, 2029–2045, https://doi.org/10.1175/1520-0450(1995)034<2029:NSOTEO>2.0.CO;2.

Crum, T. D., and R. L. Alberty, 1993: The WSR-88D and the WSR-88D Operational Support Facility. *Bull. Amer. Meteor. Soc.*, **74**, 1669–1687, https://doi.org/10.1175/1520-0477(1993)074<1669:TWATWO>2.0.CO;2.

——, ——, and D. W. Burgess, 1993: Recording, archiving, and using WSR-88D data. *Bull. Amer. Meteor. Soc.*, **74**, 645–653, https://doi.org/10.1175/1520-0477(1993)074<0645:RAAUWD>2.0.CO;2.

——, R. E. Saffle, and J. W. Wilson, 1998: An update on the NEXRAD program and future WSR-88D support to operations. *Wea. Forecasting*, **13**, 253–262, https://doi.org/10.1175/1520-0434(1998)013<0253:AUOTNP>2.0.CO;2.

Cummins, K. L., and M. J. Murphy, 2009: An overview of lightning locating systems: History, techniques, and data uses, with an in-depth look at the U.S. NLDN. *IEEE Trans. Electromagn. Compat.*, **51**, 499–518, https://doi.org/10.1109/TEMC.2009.2023450.

——, ——, E. A. Bardo, W. L. Hiscox, R. B. Pyle, and A. E. Pifer, 1998: A combined TOA/MDF technology update of the U.S. National Lightning Detection Network. *J. Geophys. Res.*, **103**, 9035–9044, https://doi.org/10.1029/98JD00153.

DeAngelis, A., F. Dominguez, Y. Fan, A. Robock, M. D. Kustu, and D. Robinson, 2010: Evidence of enhanced precipitation due to irrigation over the Great Plains of the United States. *J. Geophys. Res.*, **115**, D15115, https://doi.org/10.1029/2010JD013892.

Deierling, W., and W. A. Petersen, 2008: Total lightning activity as an indicator of updraft characteristics. *J. Geophys. Res.*, **113**, D16210, https://doi.org/10.1029/2007JD009598.

Devadoss, S. L., and J. O'Rourke, 2011: *Discrete and Computational Geometry*. Princeton University Press, 280 pp.

Diem, J. E., and T. L. Mote, 2005: Interepochal changes in summer precipitation in the southeastern United States: Evidence of possible urban effects near Atlanta, Georgia. *J. Appl. Meteor.*, **44**, 717–730, https://doi.org/10.1175/JAM2221.1.

Dixon, P. G., and T. L. Mote, 2003: Patterns and causes of Atlanta's urban heat island–initiated precipitation. *J. Appl. Meteor.*, **42**, 1273–1284, https://doi.org/10.1175/1520-0450(2003)042<1273:PACOAU>2.0.CO;2.

Dou, J., Y. Wang, R. Bornstein, and S. Miao, 2015: Observed spatial characteristics of Beijing urban climate impacts on summer thunderstorms. *J. Appl. Meteor. Climatol.*, **54**, 94–105, https://doi.org/10.1175/JAMC-D-13-0355.1.

Gallo, K. P., and T. W. Owen, 1999: Satellite-based adjustments for the urban heat island temperature bias. *J. Appl. Meteor.*, **38**, 806–813, https://doi.org/10.1175/1520-0450(1999)038<0806:SBAFTU>2.0.CO;2.

Gero, A. F., and A. J. Pitman, 2006: The impact of land cover change on a simulated storm event in the Sydney basin. *J. Appl. Meteor. Climatol.*, **45**, 283–300, https://doi.org/10.1175/JAM2337.1.

Goodman, S. J., and Coauthors, 2013: The GOES-R Geostationary Lightning Mapper (GLM). *Atmos. Res.*, **125–126**, 34–49, doi:10.1016/j.atmosres.2013.01.006.

Greene, D. R., and R. A. Clark, 1972: Vertically integrated liquid water—A new analysis tool. *Mon. Wea. Rev.*, **100**, 548–552, https://doi.org/10.1175/1520-0493(1972)100<0548:VILWNA>2.3.CO;2.

Haberlie, A. M., W. S. Ashley, and T. J. Pingel, 2015: The effect of urbanization on the climatology of thunderstorm initiation. *Quart. J. Roy. Meteor. Soc.*, **141**, 663–675, https://doi.org/10.1002/qj.2499.

Hand, L. M., and J. M. Shepherd, 2009: An investigation of warm-season spatial rainfall variability in Oklahoma City: Possible linkages to urbanization and prevailing wind. *J. Appl. Meteor. Climatol.*, **48**, 251–269, https://doi.org/10.1175/2008JAMC2036.1.

Herzog, B. S., K. M. Calhoun, and D. R. MacGorman, 2014: Total lightning information in a 5-year thunderstorm climatology. *XVth Int. Conf. on Atmospheric Electricity*, Norman, OK, International Commission on Atmospheric Electricity.

Hobson, A. G., V. Lakshmanan, T. M. Smith, and M. Richman, 2012: An automated technique to categorize storm type from radar and near-storm environment data. *Atmos. Res.*, **111**, 104–113, https://doi.org/10.1016/j.atmosres.2012.03.004.

Homer, C. G., and Coauthors, 2015: Completion of the 2011 National Land Cover Database for the conterminous United States—Representing a decade of land cover change information. *Photogramm. Eng. Remote Sensing*, **81**, 345–354.

Huff, F. A., and S. A. Changnon Jr., 1972: Climatological assessment of urban effects on precipitation at St. Louis. *J. Appl. Meteor.*, **11**, 823–842, https://doi.org/10.1175/1520-0450(1972)011<0823:CAOUEO>2.0.CO;2.

——, and ——, 1973: Precipitation modification by major urban areas. *Bull. Amer. Meteor. Soc.*, **54**, 1220–1232, https://doi.org/10.1175/1520-0477(1973)054<1220:PMBMUA>2.0.CO;2.

Jauregui, E., and E. Romales, 1996: Urban effects on convective precipitation in Mexico City. *Atmos. Environ.*, **30**, 3383–3389, https://doi.org/10.1016/1352-2310(96)00041-6.

Jing, Z., and G. Wiener, 1993: Two-dimensional dealiasing of Doppler velocities. *J. Atmos. Oceanic Technol.*, **10**, 798–808, https://doi.org/10.1175/1520-0426(1993)010<0798:TDDODV>2.0.CO;2.

Kawecki, S., G. M. Henebry, and A. L. Steiner, 2016: Effects of urban plume aerosols on a mesoscale convective system. *J. Atmos. Sci.*, **73**, 4641–4660, https://doi.org/10.1175/JAS-D-16-0084.1.

Kishtawal, C. M., D. Niyogi, M. Tewari, R. A. Pielke Sr., and J. M. Shepherd, 2010: Urbanization signature in the observed heavy rainfall climatology over India. *Int. J. Climatol.*, **30**, 1908–1916, https://doi.org/10.1002/joc.2044.

Lakshmanan, V., and T. Smith, 2009: Data mining storm attributes from spatial grids. *J. Atmos. Oceanic Technol.*, **26**, 2353–2365, https://doi.org/10.1175/2009JTECHA1257.1.

——, ——, K. Hondl, G. J. Stumpf, and A. Witt, 2006: A real-time, three-dimensional, rapidly updating, heterogeneous radar merger technique for reflectivity, velocity, and derived products. *Wea. Forecasting*, **21**, 802–823, https://doi.org/10.1175/WAF942.1.

——, A. Fritz, T. Smith, K. Hondl, and G. Stumpf, 2007a: An automated technique to quality control radar reflectivity data. *J. Appl. Meteor. Climatol.*, **46**, 288–305, https://doi.org/10.1175/JAM2460.1.

——, T. Smith, G. Stumpf, and K. Hondl, 2007b: The Warning Decision Support System–Integrated Information. *Wea. Forecasting*, **22**, 596–612, https://doi.org/10.1175/WAF1009.1.

——, K. Hondl, and R. Rabin, 2009: An efficient, general-purpose technique for identifying storm cells in geospatial images. *J. Atmos. Oceanic Technol.*, **26**, 523–537, https://doi.org/10.1175/2008JTECHA1153.1.

——, B. Herzog, and D. Kingfield, 2015: A method for extracting postevent storm tracks. *J. Applied Meteor. Climatol.*, **54**, 451–462, https://doi.org/10.1175/JAMC-D-14-0132.1.

Landsberg, C., 1981: *The Urban Climate.* Academic Press, 275 pp.

Lebo, Z. L., 2014: The sensitivity of a numerically simulated idealized squall line to the vertical distribution of aerosols. *J. Atmos. Sci.*, **71**, 4581–4596, https://doi.org/10.1175/JAS-D-14-0068.1.

Lowry, W. P., 1998: Urban effects on precipitation amount. *Prog. Phys. Geogr.*, **22**, 477–520, https://doi.org/10.1191/030913398670090480.

Maddox, R. A., D. S. Zaras, P. L. MacKeen, J. J. Gourley, R. Rabin, and K. W. Howard, 1999: Echo height measurements with the WSR-88D: Use of data from one versus two radars. *Wea. Forecasting*, **14**, 455–460, https://doi.org/10.1175/1520-0434(1999)014<0455:EHMWTW>2.0.CO;2.

Matyas, C. J., 2010: Use of ground-based radar for climate-scale studies of weather and rainfall. *Geogr. Compass*, **4**, 1218–1237, https://doi.org/10.1111/j.1749-8198.2010.00370.x.

Melillo, J. M., T. Richmond, and G. W. Yohe, Eds., 2014: *Climate Change Impacts in the United States: The Third National Climate Assessment.* U.S. Global Climate Change Research Program, 841 pp., https://doi.org/10.7930/J0Z31WJ2.

Miller, M. L., V. Lakshmanan, and T. M. Smith, 2013: An automated method for depicting mesocyclone paths and intensities. *Wea. Forecasting*, **28**, 570–585, https://doi.org/10.1175/WAF-D-12-00065.1.

Mitra, C., and J. M. Shepherd, 2016: Urban precipitation: A global perspective. *Routledge Handbook of Urbanization and Global Environmental Change*, K. C. Seto, W. D. Solecki, and C. A. Griffith, Eds., Routledge, 152–168.

——, ——, and T. Jordan, 2012: On the relationship between the premonsoonal rainfall climatology and urban land cover dynamics in Kolkata City, India. *Int. J. Climatol.*, **32**, 1443–1454, https://doi.org/10.1002/joc.2366.

Mote, T. L., M. C. Lacke, and J. M. Shepherd, 2007: Radar signatures of the urban effect on precipitation: A case study for Atlanta, Georgia. *Geophys. Res. Lett.*, **34**, L20710, https://doi.org/10.1029/2007GL031903.

Niyogi, D., T. Holt, S. Zhong, P. C. Pyle, and J. Basara, 2006: Urban and land surface effects on the 30 July 2003 mesoscale convective system event observed in the southern Great Plains. *J. Geophys. Res.*, **111**, D19107, https://doi.org/10.1029/2005JD006746.

——, P. Pyle, M. Lei, S. P. Arya, C. M. Kishtawal, M. Shepherd, F. Chen, and B. Wolfe, 2011: Urban modification of thunderstorms: An observational storm climatology and model case study for the Indianapolis urban region. *J. Appl. Meteor. Climatol.*, **50**, 1129–1144, https://doi.org/10.1175/2010JAMC1836.1.

——, M. Lei, C. Kishtawal, P. Schmid, and M. Shepherd, 2017: Urbanization impacts on the summer heavy rainfall climatology over the eastern United States. *Earth Interact.*, **21**, https://doi.org/10.1175/EI-D-15-0045.1.

NOAA/NCEI, 2014: Climatological rankings. National Oceanic and Atmospheric Administration/National Centers for Environmental Information, https://www.ncdc.noaa.gov/temp-and-precip/climatological-rankings/.

Ntelekos, A. A., J. A. Smith, and W. F. Krajewski, 2007: Climatological analyses of thunderstorms and flash floods in the Baltimore metropolitan region. *J. Hydrometeor.*, **8**, 88–101, https://doi.org/10.1175/JHM558.1.

——, ——, L. Donner, J. D. Fast, W. I. Gustafson, E. G. Chapman, and W. F. Krajewski, 2009: The effects of aerosols on intense convective precipitation in the northeastern United States. *Quart. J. Roy. Meteor. Soc.*, **135**, 1367–1391, https://doi.org/10.1002/qj.476.

Oke, T. R., 1973: City size and the urban heat island. *Atmos. Environ.*, **7**, 769–779, https://doi.org/10.1016/0004-6981(73)90140-6.

——, 1987: *Boundary Layer Climates.* 2nd ed. Routledge, 435 pp.

Polger, P. D., B. S. Goldsmith, R. C. Przywarty, and J. R. Bocchieri, 1994: National Weather Service warning performance based on the WSR-88D. *Bull. Amer. Meteor. Soc.*, **75**, 203–214, https://doi.org/10.1175/1520-0477(1994)075<0203:NWSWPB>2.0.CO;2.

Rabin, R. M., D. J. Stensrud, S. Stadler, P. J. Wetzel, and M. Gregory, 1990: Observed effects of landscape variability on convective clouds. *Bull. Amer. Meteor. Soc.*, **71**, 272–280, https://doi.org/10.1175/1520-0477(1990)071<0272:OEOLVO>2.0.CO;2.

Robaa, S. M., 2003: Urban-suburban/rural differences over greater Cairo, Egypt. *Atmósfera*, **16**, 157–171.

Rose, L. S., J. A. Stallins, and M. L. Bentley, 2008: Concurrent cloud-to-ground lightning and precipitation enhancement in the Atlanta, Georgia (United States), urban region. *Earth Interact.*, **12**, https://doi.org/10.1175/2008EI265.1.

Rosenfeld, D., U. Lohmann, G. B. Raga, C. D. O'Dowd, M. Kulmala, S. Fuzzi, and M. O. Andreae, 2008: Flood or drought: How do aerosols affect precipitation? *Science*, **321**, 1309–1313, https://doi.org/10.1126/science.1160606.

Rossum, S., and S. Lavin, 2000: Where are the Great Plains? A cartographic analysis. *Prof. Geogr.*, **52**, 543–552, https://doi.org/10.1111/0033-0124.00245.

Roth, M., 2007: Review of urban climate research in (sub)tropical regions. *Int. J. Climatol.*, **27**, 1859–1873, https://doi.org/10.1002/joc.1591.

Schaefer, J. T., and R. Edwards, 1999: The SPC Tornado/Severe Thunderstorm Database. Preprints, *11th Conf. of Applied Climatology*, Dallas, TX, Amer. Meteor. Soc., 215–220.

Schmid, P. E., and D. Niyogi, 2013: Impact of city size on precipitation-modifying potential. *Geophys. Res. Lett.*, **40**, 5263–5267, https://doi.org/10.1002/grl.50656.

——, and ——, 2017: Modeling urban precipitation modification by spatially heterogeneous aerosols. *J. Appl. Meteor. Climatol.*, **56**, 2141–2153, https://doi.org/10.1175/JAMC-D-16-0320.1.

Schmit, T. J., P. Griffith, M. M. Gunshor, J. M. Daniels, S. J. Goodman, and W. J. Lebair, 2017: A closer look at the ABI on the GOES-R series. *Bull. Amer. Meteor. Soc.*, **98**, 681–698, https://doi.org/10.1175/BAMS-D-15-00230.1.

Schultz, C. J., L. D. Carey, E. V. Schultz, and R. J. Blakeslee, 2015: Insight into the kinematic and microphysical processes that control lightning jumps. *Wea. Forecasting*, **30**, 1591–1621, https://doi.org/10.1175/WAF-D-14-00147.1.

Serafin, R. J., and J. W. Wilson, 2000: Operational weather radar in the United States: Progress and opportunity. *Bull. Amer. Meteor. Soc.*, **81**, 501–518, https://doi.org/10.1175/1520-0477(2000)081<0501:OWRITU>2.3.CO;2.

Seto, K. C., B. Güeralp, and L. R. Hutyra, 2012: Global forecasts of urban expansion to 2030 and direct impacts on biodiversity and carbon pools. *Proc. Natl. Acad. Sci. USA*, **109**, 16 083–16 088, https://doi.org/10.1073/pnas.1211658109.

Shepherd, J. M., 2005: A review of current investigations of urban-induced rainfall and recommendations for the future. *Earth Interact.*, **9**, https://doi.org/10.1175/EI156.1.

——, 2013: Impacts of urbanization on precipitation and storms: Physical insights and vulnerabilities. *Climate Vulnerability: Understanding and Addressing Threats to Essential Resources*, R. A. Pielke, Ed., Elsevier, 109–125.

——, and S. J. Burian, 2003: Detection of urban-induced rainfall anomalies in a major coastal city. *Earth Interact.*, **7**, https://doi.org/10.1175/1087-3562(2003)007<0001:DOUIRA>2.0.CO;2.

——, H. Pierce, and A. J. Negri, 2002: Rainfall modification by major urban areas: Observations from spaceborne rain radar on the TRMM satellite. *J. Appl. Meteor.*, **41**, 689–701, https://doi.org/10.1175/1520-0450(2002)041<0689:RMBMUA>2.0.CO;2.

Sheridan, S. C., 2002: The redevelopment of a weather-type classification scheme for North America. *Int. J. Climatol.*, **22**, 51–68, https://doi.org/10.1002/joc.709.

Singh, J., H. Vittal, S. Karmakar, S. Ghosh, and D. Niyogi, 2016: Urbanization causes nonstationarity in Indian summer monsoon rainfall extremes. *Geophys. Res. Lett.*, **43**, 11 269–11 277, https://doi.org/10.1002/2016GL071238.

Smith, B. T., R. L. Thompson, J. S. Grams, C. Broyles, and H. E. Brooks, 2012: Convective modes for significant severe thunderstorms in the contiguous Unites States. Part I: Storm classification and climatology. *Wea. Forecasting*, **27**, 1114–1135, https://doi.org/10.1175/WAF-D-11-00115.1.

Smith, J. A., A. A. Bradley, and M. L. Baeck, 1994: The space–time structure of extreme storm rainfall in the southern plains. *J. Appl. Meteor.*, **33**, 1402–1417, https://doi.org/10.1175/1520-0450(1994)033<1402:TSSOES>2.0.CO;2.

——, M. L. Baeck, G. Villarini, C. Welty, A. J. Miller, and W. F. Krajewski, 2012: Analyses of a long-term, high-resolution radar rainfall data set for the Baltimore metropolitan region. *Water Resour. Res.*, **48**, W04504, https://doi.org/10.1029/2011WR010641.

Smith, T. M., and K. L. Elmore, 2004: The use of radial velocity derivatives to diagnose rotation and divergence. *11th Conf. on Aviation, Range, and Aerospace*, Hyannis, MA, Amer. Meteor. Soc., P5.6, https://ams.confex.com/ams/pdfpapers/81827.pdf.

——, and Coauthors, 2016: Multi-Radar Multi-Sensor (MRMS) severe weather and aviation products: Initial operating capabilities. *Bull. Amer. Meteor. Soc.*, **97**, 1617–1630, https://doi.org/10.1175/BAMS-D-14-00173.1.

Souch, C., and S. Grimmond, 2006: Applied climatology: Urban climate. *Prog. Phys. Geogr.*, **30**, 270–279, https://doi.org/10.1191/0309133306pp484pr.

Stallins, J. A., and L. S. Rose, 2008: Urban lightning: Current research, methods, and the geographical perspective. *Geogr. Compass*, **2**, 620–639, https://doi.org/10.1111/j.1749-8198.2008.00110.x.

——, M. Bentley, and L. S. Rose, 2006: Cloud-to-ground flash patterns for Atlanta, Georgia (USA) from 1992 to 2003. *Climate Res.*, **30**, 99–112, https://doi.org/10.3354/cr030099.

Steiger, S. M., R. E. Orville, and G. Huffines, 2002: Cloud-to-ground lightning characteristics over Houston, Texas: 1989–2000. *J. Geophys. Res.*, **107**, 4117, https://doi.org/10.1029/2001JD001142.

Tayanc, M., and H. Toros, 1997: Urbanization effects on regional climate change in the case of four large cities of Turkey. *Climatic Change*, **35**, 501–524, https://doi.org/10.1023/A:1005357915441.

Torres, S. M., and C. D. Curtis, 2007: Initial implementation of super-resolution data on the NEXRAD network. *23rd Conf. on Interactive Information Processing Systems*, San Antonio, TX, Amer. Meteor. Soc., 5B.10, https://ams.confex.com/ams/87ANNUAL/techprogram/paper_116240.htm.

United Nations, 2014: World urbanization prospects: The 2014 revision. Department of Economic and Social Affairs, United Nations, New York, NY, 32 pp., https://esa.un.org/unpd/wup/publications/files/wup2014-highlights.pdf.

U.S. Census Bureau, 2010: Census urban and rural classification and urban area criteria. U.S. Census Bureau, http://www.census.gov/geo/reference/ua/urban-rural-2010.html.

Van den Heever, S. C., and W. R. Cotton, 2007: Urban aerosol impacts on downwind convective storms. *J. Appl. Meteor. Climatol.*, **46**, 828–850, https://doi.org/10.1175/JAM2492.1.

Walker, J. J., K. M. de Beurs, and G. M. Henebry, 2015: Land surface phenology along urban to rural gradients in the U.S. Great Plains. *Remote Sens. Environ.*, **165**, 42–52, https://doi.org/10.1016/j.rse.2015.04.019.

Westcott, N. E., 1995: Summertime cloud-to-ground lightning activity around major midwestern urban areas. *J. Appl. Meteor.*, **34**, 1633–1642, https://doi.org/10.1175/1520-0450-34.7.1633.

Wilks, D. S., 1995: *Statistical Methods in the Atmospheric Sciences: An Introduction*. Academic Press, 467 pp.

Witt, A., M. D. Eilts, G. J. Stumpf, J. T. Johnson, E. D. Mitchell, and K. W. Thomas, 1998: An enhanced hail detection algorithm for the WSR-88D. *Wea. Forecasting*, **13**, 286–303, https://doi.org/10.1175/1520-0434(1998)013<0286:AEHDAF>2.0.CO;2.

Yonetani, T., 1982: Increase in number of days with heavy precipitation in Tokyo urban area. *J. Appl. Meteor.*, **21**, 1466–1471, https://doi.org/10.1175/1520-0450(1982)021<1466:IINODW>2.0.CO;2.

Zhang, Y., J. A. Smith, L. Luo, Z. Wang, and M. L. Baeck, 2014: Urbanization and rainfall variability in the Beijing metropolitan region. *J. Hydrometeor.*, **15**, 2219–2235, https://doi.org/10.1175/JHM-D-13-0180.1.

Zrnić, D.S. and A.V. Ryzhkov, 1999: Polarimetry for weather surveillance radars. *Bull. Amer. Meteor. Soc.*, **80**, 389–406, https:doi.org/10.1175/1520-0477(1999)080<0389:PFWSR>2.0.CO;2.